The Plant Cell, Vol. 25: 3910–3925, October 2013, www.plantcell.org

Mediation of Clathrin-Dependent Trafficking during Cytokinesis and Cell Expansion by *Arabidopsis* STOMATAL CYTOKINESIS DEFECTIVE Proteins[W]

Colleen M. McMichael,[a,1] Gregory D. Reynolds,[a,1] Lisa M. Koch,[a,2] Chao Wang,[b] Nan Jiang,[b] Jeanette Nadeau,[c] Fred D. Sack,[c,d] Max B. Gelderman,[a,3] Jianwei Pan,[b] and Sebastian Y. Bednarek[a,4]

[a] Department of Biochemistry, University of Wisconsin-Madison, Madison, Wisconsin 53706
[b] College of Chemistry and Life Sciences, Zhejiang Normal University, Zhejiang 321004, China
[c] Department of Plant Biology, Ohio State University, Columbus, Ohio 43210
[d] Department of Botany, University of British Columbia, Vancouver, British Columbia V6T 1Z4, Canada

***STOMATAL CYTOKINESIS DEFECTIVE1* (*SCD1*) encodes a putative Rab guanine nucleotide exchange factor that functions in membrane trafficking and is required for cytokinesis and cell expansion in *Arabidopsis thaliana*. Here, we show that the loss of *SCD2* function disrupts cytokinesis and cell expansion and impairs fertility, phenotypes similar to those observed for *scd1* mutants. Genetic and biochemical analyses showed that SCD1 function is dependent upon SCD2 and that together these proteins are required for plasma membrane internalization. Further specifying the role of these proteins in membrane trafficking, SCD1 and SCD2 proteins were found to be associated with isolated clathrin-coated vesicles and to colocalize with clathrin light chain at putative sites of endocytosis at the plasma membrane. Together, these data suggest that SCD1 and SCD2 function in clathrin-mediated membrane transport, including plasma membrane endocytosis, required for cytokinesis and cell expansion.**

INTRODUCTION

In plants, cytokinesis is mediated by the de novo assembly of the cell plate (CP) that forms a new cell wall (CW) and plasma membrane (PM). Beginning in late anaphase, secretory vesicles deliver lipids, proteins, and CW materials to the division plane and then fuse to initiate CP construction. Continued vesicle delivery and fusion drive centrifugal expansion and maturation of the CP (McMichael and Bednarek, 2013). Following cytokinesis, plant cells expand through, for example, diffuse or tip-directed growth. Plant cell expansion, which determines cell shape and ultimately plant morphology, is accomplished by the polarized targeting and localized release of secretory pathway-derived membrane and CW materials at specific sites on the PM (Smith, 2003).

Polarized delivery of endomembrane-derived vesicles during CP formation and cell expansion is balanced by retrieval of membrane and proteins via clathrin-mediated endocytosis (CME) (McMichael and Bednarek, 2013). Thus, while cytokinesis and cell expansion are temporally distinct processes, they appear to rely on similar molecular machinery. Indeed, both processes are highly dependent upon endomembrane trafficking to add new membrane and CW materials to an expanding CP or the existing PM. Numerous membrane transport and fusion proteins function in both cytokinesis and cell expansion. For example, the *Arabidopsis thaliana* small GTPase RabA2a is necessary for delivery of *trans*-Golgi network (TGN)–derived vesicles to the PM during tip-directed expansion of pollen tubes and to the leading edge of the CP during cytokinesis (de Graaf et al., 2005; Chow et al., 2008).

To date, various plant cytokinesis-defective mutants have been identified that manifest multinucleate cells harboring incomplete transverse CW inclusions. These mutants fall into several distinct classes depending on the processes disrupted and include plants dysfunctional in cytoskeletal dynamics (e.g., loss-of-function or dominant-negative *formin homology* mutants; Deeks et al., 2005; Ingouff et al., 2005; Ye et al., 2009; Cheung et al., 2010; Li et al., 2010), membrane transport and fusion (e.g., *dynamin related protein1* [*drp1*] and *tplate*; Kang et al., 2003a, 2003b; Van Damme et al., 2006, 2011; Collings et al., 2008), or CW biogenesis (*massue* [*mas*]/*glucan synthase like8* [*gsl8*]/*chorus* [*chor*]; Chen et al., 2009; Thiele et al., 2009; Guseman et al., 2010). In addition to cytokinesis defects, many of these mutants display atypical cell expansion that results in smaller, abnormally shaped, or even swollen cells and/or disorganized cell patterning that results in irregular tissue and organ structures (reviewed in Backues et al., 2007; McMichael and Bednarek, 2013).

Stomata, specialized plant epidermal gas-exchanging structures, consist of a pore surrounded by a pair of guard cells (GCs), the daughter cells resulting from the symmetric division of a guard mother cell (GMC). In *Arabidopsis*, this terminal symmetric division is preceded by a series of asymmetric divisions in which a meristemoid mother cell divides unequally to produce a small meristemoid that may continue to divide asymmetrically or directly

[1] These authors contributed equally to this work.
[2] Current address: U.S. Dairy Forage Research Center, 1925 Linden Drive West, Madison, WI 53706.
[3] Current address: Ecolab, 940 Lone Oak Road, Eagan, MN 55121.
[4] Address correspondence to sybednar@wisc.edu.
The author responsible for distribution of materials integral to the findings presented in this article in accordance with the policy described in the Instructions for Authors (www.plantcell.org) is: Sebastian Y. Bednarek (sybednar@wisc.edu).
[W] Online version contains Web-only data.
www.plantcell.org/cgi/doi/10.1105/tpc.113.115162

form an oval-shaped GMC (Nadeau, 2009). The stereotyped shape and division of the GMC facilitates the microscopy-based identification of nonlethal *Arabidopsis* mutants that disrupt cytokinesis, including *cytokinesis defective1* (*cyd1*; Yang et al., 1999), *stomatal cytokinesis defective1* (*scd1*; Falbel et al., 2003), and *scd2* (see below). In the temperature-sensitive *scd1-1* mutant, cytokinesis of the GMC is disrupted when plants are grown above the permissive temperature range of 15 to 18°C, resulting in a missing or partial GC wall. While the cytokinesis-defective phenotype of *scd1-1* predominantly manifests in GCs, cytokinesis of epidermal pavement cells is affected as well (Falbel et al., 2003). *scd1-1* and loss-of-function *scd1-2* plants also display defects in overall growth and development; they are stunted in both aerial structures and roots, are infertile (Falbel et al., 2003), and have increased bacterial pathogen resistance (Korasick et al., 2010) compared with the wild type.

The predicted 131.5-kD SCD1 protein includes an N-terminal, tripartite differentially expressed in normal and neoplastic cells domain (DENN; Levivier et al., 2001) and eight C-terminal WD-40 repeats (WD-40 repeats span 40 to 60 residues that typically terminate with a Trp-Asp [WD] motif) (Falbel et al., 2003). Animal DENN proteins have been shown to function as Rab guanine nucleotide exchange factors (GEFs), which activate Rabs by stimulating release of GDP and binding of GTP (Grosshans et al., 2006; Yoshimura et al., 2010). In particular, connecdenn 1, 2, and 3/DENND1A, B, and C are clathrin-coated vesicle (CCV)–associated GEFs for Rab35 (Allaire et al., 2010; Marat and McPherson, 2010), which functions in CCV trafficking, endosomal recycling, actin regulation, and cytokinesis in animals (Kouranti et al., 2006; Patino-Lopez et al., 2008; Sato et al., 2008; Zhang et al., 2009).

In plants, CME is recognized as the major endocytic mechanism and is necessary for proper plant growth, development, and signaling (Dhonukshe et al., 2007; Robert et al., 2010; Kitakura et al., 2011; Adam et al., 2012; Wang et al., 2013). Clathrin oligomers and CCV cargoes are assembled on source membranes through their association with heterotetrameric adaptin protein (AP) scaffolding complexes. In plant and animal systems, AP2 and AP1 are the major PM-associated CME and TGN-associated clathrin-mediated membrane recycling vesicle adaptors, respectively (Kirchhausen, 2000; Bashline et al., 2013; Di Rubbo et al., 2013; Fan et al., 2013; Kim et al., 2013; Teh et al., 2013; Park et al., 2013; Wang et al., 2013; Yamaoka et al., 2013). Plant genomes also encode many clathrin-associated sorting proteins (CLASPs) that aid adaptin-mediated formation of CCVs, including AP180/epsin N-terminal homology (A/ENTH) domain proteins and dynamin-related proteins (DRPs) that facilitate membrane curvature and vesicle scission, respectively (Chen et al., 2011). Clathrin, A/ENTH domain proteins, DRPs, and the adaptin-related TPLATE have also been detected at the CP (Konopka and Bednarek, 2008a; Konopka et al., 2008; Fujimoto et al., 2010; Van Damme et al., 2011; Ito et al., 2012; Song et al., 2012), suggesting that a mechanism similar to CME and clathrin-mediated membrane retrieval at the TGN facilitates membrane recycling from the CP during plant cytokinesis.

Here, we describe the identification of the *Arabidopsis scd2* mutant and the characterization of its cytokinesis and cell expansion defects, which are similar to those of *scd1*, namely, dwarfed and infertile plants with observable epidermal cytokinesis failures. Phenotypic and protein expression analyses of *scd1* and *scd2* single and double mutants suggest that SCD1 functions upstream of SCD2. Furthermore, SCD1 and SCD2 proteins were found to be associated with isolated CCVs and with clathrin-coated pits (CCPs) at the PM. Consistent with their role in CME, *scd1* and *scd2* mutants displayed impaired FM4-64 internalization. Together, these data suggest that SCD1 and SCD2 function in clathrin-mediated membrane trafficking essential to both cytokinesis and cell expansion.

RESULTS

Isolation and Phenotypic Analysis of *scd2* Mutants

Heterozygous *scd2-1*/+ plants segregated for defects in plant growth and development as expected for a single recessive mutation (139 mutant:373 wild type, $\chi^2 = 1.26$, $P = 0.262$). Analysis of fully expanded mature rosette leaves revealed cytokinesis defects in ~58% of *scd2-1* stomata, representing the various types of defects (oblate/type 2, stub/type 3, and hanging pore/type 4) observed in the stomatal cytokinesis-defective mutants *scd1-1* (Falbel et al., 2003) and *cyd1* (Yang et al., 1999) (Figures 1A to 1D, 1F to 1I, 1J to 1M, and 1O to 1R). Oblate/type 2 stomata, in which no ventral wall or pore was evident (Figures 1B, 1G, 1K, and 1P), predominated at 50%, and stomata containing one or more incomplete ventral wall(s) (stub/type 3; Figures 1C, 1H, 1L, and 1Q), including those that contained a pore (hanging pore/type 4; Figures 1D, 1I, 1M, and 1R), occurred at ~8% frequency. Similar to *scd1-1* mutants (Falbel et al., 2003), CW stubs were also observed in *scd2-1* leaf epidermal pavement cells stained with toluidine blue-O (TBO) (Figure 1E) or propidium iodide (PI) (Figure 1S) or expressing the cell surface marker green fluorescent protein–LOW TEMPERATURE-INDUCED 6b (GFP-LTI6b; Cutler et al., 2000) (Figure 1N), albeit less frequently than in stomata. The GC-specific reporter fusion *POTASSIUM CHANNEL IN ARABIDOPSIS THALIANA1*$_{pro}$–bacterial β-glucuronidase (*KAT1*$_{pro}$*-GUS*; Nakamura et al., 1995) was used to confirm the GC identity of oblate stomata in *scd2-1* leaves, distinguishing them from cell cycle–arrested GMCs (Figures 1F to 1I). Additionally, defective *scd2-1* stomata expressing the N7 nuclear GFP (Cutler et al., 2000) were observed by confocal laser scanning microscopy (CLSM) to be binucleate (Figures 1O to 1R), an indicator of normal karyokinesis despite subsequent defective cytokinesis. The stomatal density in *scd2-1* leaves was elevated (173 ± 15.3 GC/mm^2; $n = 11$) relative to that in wild-type leaves (143 ± 8.42 GC/mm^2; $n = 4$ ± SE).

Additional phenotypes, such as incongruous spaces or gaps between epidermal cells and clusters of small cells, were observed in the epidermis of *scd2-1* leaves and cotyledons when analyzed by CLSM (see Supplemental Figure 1A online). The spaces/gaps were readily visualized by CLSM in cotyledons from plants expressing GFP-LTI6b 6 d after germination (DAG) as small regions between adjacent cells that densely stained with PI and appeared not to be bound by a distinct PM (see Supplemental Figures 1C to 1E online). Clusters of small cells arranged more or less symmetrically were also observed in the cotyledon epidermis of PI-stained and GFP-LTI6b–expressing

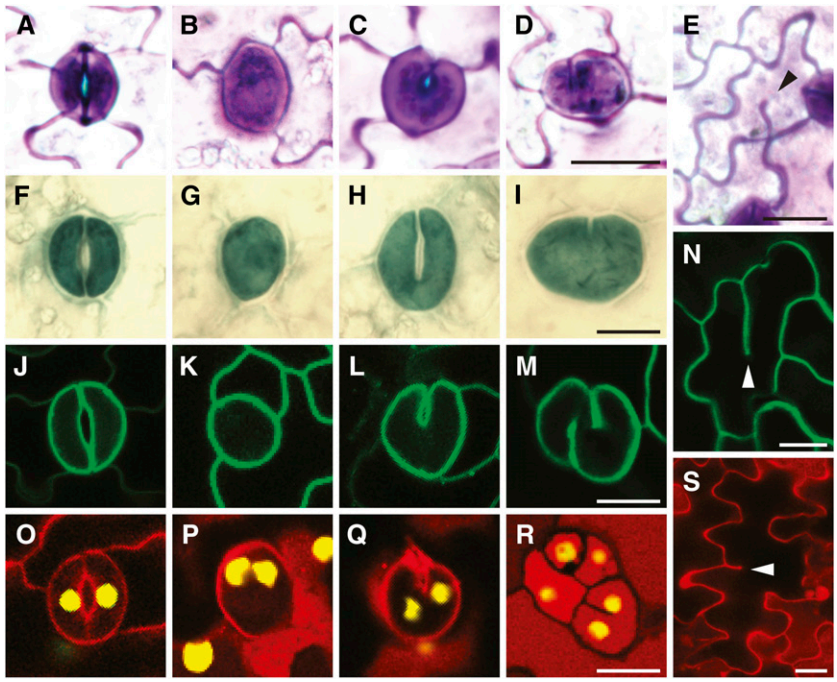

Figure 1. Cytokinesis Defects in *scd2* Cotyledon and Leaf Epidermis.

(A) to **(E)** TBO-stained *scd2-1* leaf epidermal peels.
(F) to **(I)** GUS-stained leaf epidermis of *scd2-1* plants expressing the GC identity marker $KAT1_{pro}$-*GUS*.
(J) to **(N)** Confocal laser scanning micrographs of *scd2-1* expressing the fluorescently tagged cell surface fusion protein GFP-LTI6b.
(O) to **(S)** Confocal laser scanning micrographs of *scd2-1* expressing the N7 nuclear GFP marker and stained with PI to visualize CWs.
Stomatal morphology defects in *scd2* mutants include type 2/oblate (**[B]**, **[G]**, **[K]**, and **[P]**), type 3/ hanging pore (**[C]**, **[H]**, **[L]**, and **[Q]**), and type 4/stub (**[D]**, **[I]**, **[M]**, and **[R]**) types. Normal stomata also develop (**[A]**, **[F]**, **[J]**, and **[O]**). CW stubs are also observed in epidermal pavement cells (**[E]**, **[N]**, and **[S]**, arrowheads). Bars = 10 μm.

scd2-1 plants 6 DAG (see Supplemental Figures 2A to 2D online). The spaces/gaps and small cell clusters were previously not reported for *scd1* mutants; however, given the similarity in leaf cell division and expansion defects between *scd2* and *scd1* mutants, we reexamined the cellular arrangements observed in *scd1-2* loss-of-function mutants. Similar to *scd2-1*, CLSM imaging of PI-stained *scd1-2* cotyledons 6 DAG revealed the presence of both PI-positive spaces and small, nearly symmetrically organized, cell clusters (see Supplemental Figures 1A, 1B, and 2E to 2H online).

In addition to cytokinesis defects, *scd2-1* plants, like *scd1* mutants, displayed aberrant growth and development (Figure 2; Falbel et al., 2003). Aerial organs of *scd2-1* mutant plants were dwarfed relative to the wild type (Figures 2A to 2C), with bolts that grew to a maximum height of 3 cm (Figure 2C) and produced flowers that failed to fully mature and were infertile (Figures 2C and 2D). *scd2-1* roots were also stunted due at least in part to reduced cell numbers within the root division and transition zones (as defined in Verbelen et al., 2006) (Figures 2A and 2E). The number of cortical cells comprising these zones in three representative confocal images of PI-stained vertically grown seedlings seven DAG was 4.2 ± 0.48 cells in the division zone of *scd2-1* versus 18 ± 0.45 cells for the wild type, and in the transition zone, 5.5 ± 0.34 cells for *scd2-1* compared with 10 ± 0.86 cells for the wild type ($n = 3$ for each genotype ± SE). Cell expansion defects were also observed in both *scd1* (Falbel et al., 2003) and *scd2* mutants. The average surface area of cotyledon pavement cells from seedlings seven DAG was 46.3 ± 3.9 mm^2 in wild-type plants but only 30.4 ± 1.5 for *scd2-1* mutants ($n = 4$ [≥ 7 cells per individual] for each genotype ± SE). Unlike *scd1* mutants (Falbel et al., 2003), root hair morphology was unaffected in *scd2* seedlings (see Supplemental Figures 3B to 3D online). Like *scd1* mutants, *scd2* mutant seedlings were hypersensitive to Suc, resulting in a markedly smaller and darker appearance than wild-type seedlings grown on the same media (Falbel et al., 2003; see Supplemental Figure 3A online). Taken together, these defective phenotypes of *scd2* mutants indicate a role for SCD2 in cytokinesis and cell expansion.

Mapping, Cloning, and Expression Analysis of *SCD2*

Standard map-based cloning coupled with DNA sequencing revealed the *scd2-1* lesion to be a deletion of a guanine nucleotide at position 1372 of the At3g48860 open reading frame (ORF) (see Supplemental Figure 4 and Supplemental Methods 1 and 2 online). The identity of *SCD2* was supported through the ability of a genomic clone including the entire 4.6-kb region of At3g48860 plus 1.3 kb of upstream sequence and 0.5 kb of downstream sequence ($SCD2_{pro}$-*SCD2*) to rescue *scd2-1* mutant phenotypes. Transgenic *SCD2*/*scd2* lines displayed normal growth and development, including leaf and root expansion (Figure 3A) and

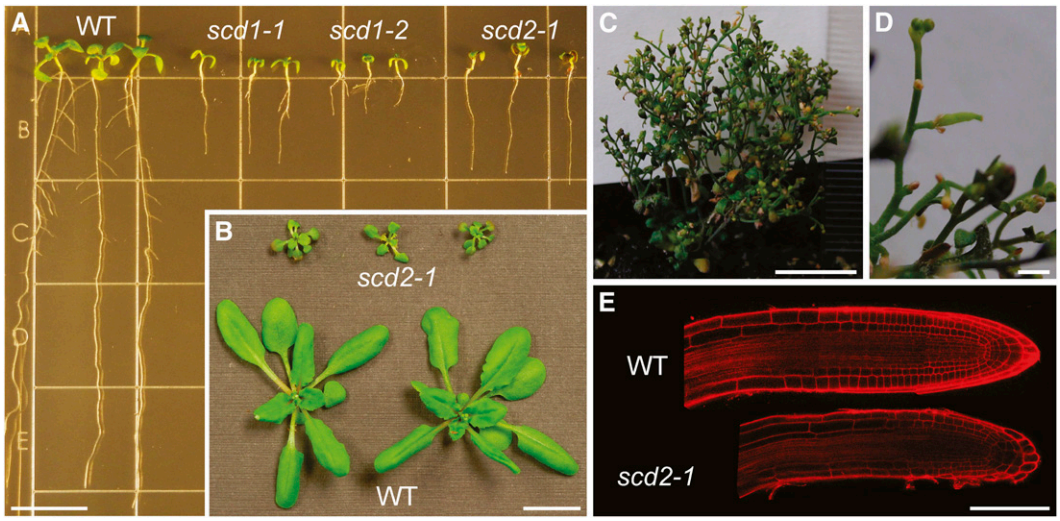

Figure 2. Growth and Cell Expansion Defects of *scd2* Mutants.

(A) Similar to *scd1* mutants, *scd2* seedlings showed reduced root and shoot elongation compared with Col-0 and Col-5 wild type [WT] when grown vertically on solid media supplemented with Suc. Bar = 10 mm.
(B) Comparison of the rosette sizes of soil-grown *scd2* and Col-5 (WT) plants 4 weeks after germination. Bar = 10 mm.
(C) Short, bushy, flowering, soil-grown *scd2* plants 14 weeks after germination. Bar = 10 mm.
(D) Close-up view of underdeveloped, infertile flowers of mature *scd2* plants (as in **[C]**). Bar = 1 mm.
(E) Comparison of confocal laser scanning micrograph composites of PI-stained roots from *scd2* and Col-5 (WT) seedlings grown vertically on solid media 7 DAG. Bar = 100 μm.

GC formation (Figures 3B to 3D), at all stages of development. In addition, a second mutant allele, *scd2-2*, which is the result of a T-DNA insertion within the third intron of *SCD2* (see Supplemental Figure 4B online), was identified that cosegregates with *scd2* mutant phenotypes.

According to data compiled by the Bio-Array Resource for Plant Functional Genomics (http://bar.utoronto.ca; Winter et al., 2007), *SCD2* is expressed in *Arabidopsis* roots, hypocotyls, cotyledons, rosette leaves, whole flowers, carpels, stamens, pollen, and seed. *SCD2* is also highly expressed in GCs (http://www.biology.ucsd.edu/labs/schroeder/guardcellchips.html; Leonhardt et al., 2004). To further assess the cell- and tissue-specific expression patterns of *SCD2*, we generated transgenic wild-type lines transformed with a bacterial *GUS*-encoding reporter ORF under control of the 1.3-kb SCD2 promoter region ($SCD2_{pro}$-*GUS*). Expression of $SCD2_{pro}$-*GUS* was observed in GCs in the epidermis of cotyledons and rosette leaves in seedlings and adult plants (Figures 4A and 4B) and often in the socket cells surrounding the base of trichomes (Figure 4B, inset). Strong GUS staining was also observed in hydathodes of fully expanded rosette leaves (Figure 4B, arrows). In roots, GUS staining was observed at the mature region of the primary root (Figure 4A) and the tips of short, young lateral roots branching from the primary root (Figures 4C and 4D), but not the primary root tip (Figure 4A).

The SCD2 Protein

SCD2 was predicted by the Pfam database (http://pfam.sanger.ac.uk/; Punta et al., 2012) to encode a 1734-bp mRNA and a 577–amino acid protein with a molecular mass of 63.74 kD containing a pair of central coiled-coil domains that mapped to Ser205-Lys268 and Gln279-Val347 (see Supplemental Figure 4C and Supplemental Methods 3 online) according to the Paircoil2 algorithm (McDonnell et al., 2006). The single base pair deletion in *scd2-1* resulted in a frame shift in the predicted ORF that would encode a truncated protein due to a premature stop codon (see Supplemental Figure 4C online) preceded by 36 out-of-frame amino acids following Leu457 of SCD2. SCD2 is similar at the amino acid level to four other *Arabidopsis* putative proteins encoded by At5g13260, At4g25070, At5g23700, and At4g08630 (see Supplemental Tables 1 and 2 and Supplemental Figure 5 online). These homologs were also predicted to encode coiled-coil domains as well as a ProDom-defined, plant-specific domain of unknown function, PD147848 (http://prodom.prabi.fr/prodom/current/html/home.php; Servant et al., 2002), at their carboxy-termini that they share with SCD2, which we refer to as the SCD2 domain (see Supplemental Table 1 and Supplemental Figure 5 online). The percentage identity and similarity of the predicted full-length proteins and SCD2 domains of these four homologs compared pairwise to SCD2 are reported in Supplemental Table 2 online. A BLAST search of the National Center for Biotechnology Information database (http://blast.ncbi.nlm.nih.gov/Blast.cgi) revealed the presence of putative SCD2 homologs in other divergent plant genomes, such as those of the genera *Ricinus* (castor), *Vitis* (grape), *Cucumis* (cucumber), *Solanum* (tomato), *Zea* (maize), *Glycine* (soybean), *Oryza* (rice), *Sorghum*, *Panicum* (switchgrass), *Picea* (spruce), and *Populus* (poplar), but not in the genomes of animals, fungi, or protists, suggesting that the SCD2 protein serves

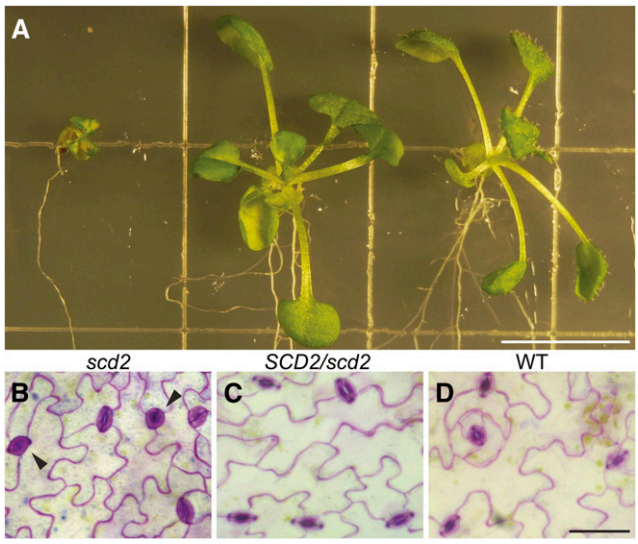

Figure 3. Genetic Rescue of *scd2-1*.

Homozygous *scd2-1* plants expressing the $SCD2_{pro}$-*SCD2* transgene resemble wild-type plants.
(A) Seedlings grown vertically on solid media supplemented with Suc. *scd2-1* seedlings (*scd2*, left) are dwarfed, while *scd2-1* rescued with the $SCD2_{pro}$-*SCD2* transgene (*SCD2*/*scd2*, center) appear indistinguishable from Col-0 (wild type [WT], right). Bar = 10 mm.
(B) to **(D)** Stomatal cytokinesis defects (arrowheads) are observed in TBO-stained epidermal peels of *scd2-1* cotyledons **(B)**. The *scd2-1* cotyledon stomatal cytokinesis defects rescued with the $SCD2_{pro}$-*SCD2* transgene **(C)** appear identical to Col-0 (**[D]**, WT). Bar = 50 μm.

a plant-specific function. Of the four *Arabidopsis* SCD2 homologs, expressed sequence tags have been identified for At5g13260, At4g25070, and At5g23700 (www.Arabidopsis.org), and all four have been detected in cDNA libraries used in microarray analyses (www.Arabidopsis.org; http://bar.utoronto.ca; Winter et al., 2007).

SCD1 and SCD2 Function in a Common Pathway

scd2 mutants share many of the pleiotropic phenotypes of *scd1* mutants, such as incomplete cytokinesis in leaf epidermal cells, cell expansion defects, and Suc hypersensitivity (Figures 1, 2 and 4; Falbel et al., 2003). Double mutant analysis was conducted to investigate whether *scd1* and *scd2* mutants affect the same or related cellular mechanisms or pathways. The root expansion defects of *scd1* and *scd2* mutant seedlings grown vertically on 1% (w/v) Suc media were visibly polymorphic and easily scored (Figure 2A); thus, root growth was monitored in a segregating *scd1-2 scd2-1* double mutant population (Figure 5). The root lengths of homozygous *scd1-2 scd2-1* double mutant and *scd1-2* and *scd2-1* single mutant seedlings 48 DAG were 19.65 ± 0.92, 16.09 ± 1.03, and 40.84 ± 0.75 mm, respectively, while the root length of wild-type seedlings, which outgrew the plate at 16 DAG, was last recorded at 75.88 ± 0.55 mm ($n = 3$ for each genotype; ±SE) (Figure 5). *scd1-2 scd2-1* and *scd1-2* root length measurements were determined not to be significantly different (Student's *t* test with $\alpha = 0.05$), and the growth rate of *scd1-2 scd2-1* double mutant seedlings was nearly identical to that of *scd1-2* mutants, while *scd2-1* and wild-type seedlings grew faster (Figure 5), indicating that *scd1-2 scd2-1* double mutants mimic the root growth phenotype of the *scd1-2* single mutants, but not that of the *scd2-1* single mutants. The *scd1-2 scd2-1* double mutant root growth phenotype also was not intermediate between (i.e., synergistic) or different from (i.e., neomorphic) that of the *scd2-1* and *scd1-2* single mutants. Together, these data indicate that *SCD1* is epistatic to *SCD2*.

Affinity-purified antibodies generated against the amino-terminus of SCD2 (anti-$SCD2^{N\text{-}term}$) reproducibly detected two polypeptides in whole seedling extracts that migrated at or near the predicted ~64-kD molecular mass of the SCD2 protein (Figure 6). Both polypeptides were absent in *scd2-1* and *scd2-2* protein extracts (Figure 6, lanes 5 and 6), while SCD2 was detected in extracts from *scd1-1* and *scd1-2* mutants at levels similar to those of the

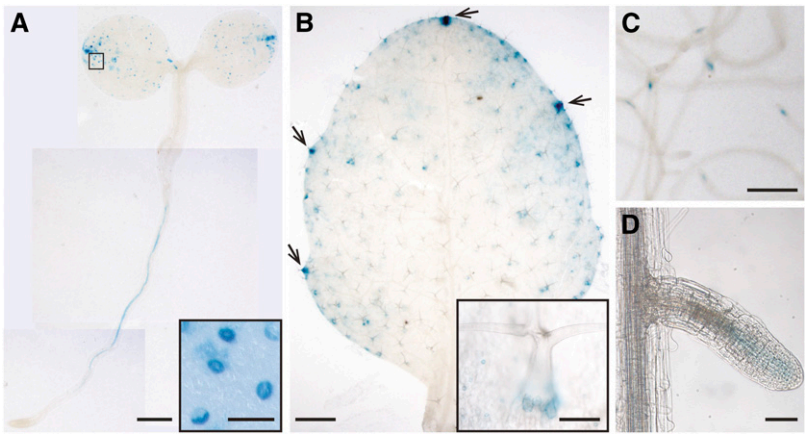

Figure 4. Histochemical Localization of $SCD2_{pro}$-*GUS* Reporter Expression.

(A) *SCD2pro-GUS*/Col-2 seedlings 3 DAG. Inset: Detail of boxed area in **(A)**. Bars = 200 μm in **(A)** and 50 μm in inset.
(B) Fully expanded *SCD2pro-GUS*/Col-2 rosette leaf. Arrows indicate strongly staining hydathodes. Inset, detail of trichome socket cells. Bars = 1 mm in **(B)** and 200 μm in inset.
(C) and **(D)** *SCD2pro-GUS*/Col-2 roots **(C)**. Phase contrast image of lateral root tip **(D)**. Bars = 200 μm in **(C)** and 50 μm in **(D)**.

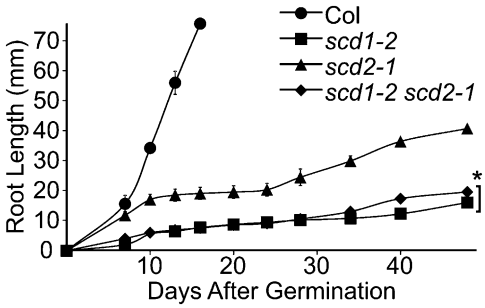

Figure 5. The Root Expansion Defects of *scd1 scd2* Double Mutants Resemble Those of *scd1*.

Measurement of the primary root growth rates of the Col-0 wild type (Col) and *scd1-2*, *scd2-1*, and *scd1-2 scd2-1* mutants grown vertically on solid media supplemented with Suc indicated that *scd1-2* and *scd1-2 scd2-1* have nearly identical growth rates. Seedlings were transferred to new media at 25 DAG. The final root length measurements taken at 48 DAG for *scd1-2* and *scd1-2 scd2-1* were not statistically different (asterisk) as determined by Student's *t* test (α = 0.05). n = 3 for each ecotype/genotype; ±SE

wild type (Columbia-5 [Col-5] and Columbia-0 [Col-0]) and *scd1* and *scd2* mutants expressing functional *SCD1* and *SCD2* under the control of their native promoters (*SCD1/scd1* and *SCD2/scd2*), respectively (Figure 6). To confirm equal loading of total protein, the samples were probed with antibodies against soluble and membrane protein markers cytosolic FRUCTOSE-1,6-BISPHOSPHATASE (cFBP) and KNOLLE (KN)/Sec12p-like protein (SEC12), respectively. As shown in Figure 6 (bottom panel), the levels of cFBP (Strand et al., 2000) were similar in all protein extracts analyzed. However, the levels of KN, a protein required for CP membrane fusion (Lauber et al., 1997), and SEC12, an integral endoplasmic reticulum membrane protein (Bar-Peled and Raikhel, 1997), varied significantly between wild-type, rescued lines, and *scd* mutant total protein extracts. These variations may reflect changes in membrane composition and/or protein abundance in the mutant plants. Indeed, a survey of *Arabidopsis* expression data available through Genevestigator (Hruz et al., 2008) for conditions that result in similar trends in KN and SEC12 expression levels indicated that the levels of these membrane-associated proteins are altered in plants challenged with a variety of biotic and abiotic stressors (e.g., pathogen elicitation, heat, and drought) and thus may be an indirect effect of the compromised development of these mutants.

As previously demonstrated (Korasick et al., 2010), affinity-purified SCD1 antibodies (anti-SCD1^{DENN}) detected the ~140-kD SCD1 protein in total protein extracts from the wild type, *SCD1/scd1*, *SCD2/scd2*, and, to a lesser extent, *scd1-1* plants, but not in *scd1-2* plant extracts (Figure 6). Interestingly, SCD1 levels were markedly reduced in total protein extracts from *scd2-1* and *scd2-2* plants compared with those of the wild type (Figure 6). By contrast, the levels of the SCD1 and SCD2 proteins were similar in plant extracts from the wild type and the stomatal cytokinesis-defective *cyd1* mutant (Yang et al., 1999), indicating that the observed reduction of SCD1 in *scd2* mutants is not due to a general defect in GC cytokinesis and cell expansion (Figure 6).

SCD1 and SCD2 Associate with CCVs

The mammalian connecdenn 1 protein has been identified as a component of CCVs (Allaire et al., 2006, 2010). To investigate if SCD1 and/or SCD2 are associated with plant CCVs, we employed a tandem fractionation scheme to prepare an enriched sample of CCVs from rapidly dividing and expanding suspension-cultured *Arabidopsis* T87W cells (Figure 7). By negative-stain electron microscopy (EM) analysis, the final CCV-enriched fraction was found to contain 76% ± 10% (n = 11) clathrin-coated versus noncoated vesicles (Figure 7B; see Supplemental Figure 6D online). Immunoblot analysis of the T87W cell lysate (H) and subsequent successive fractions generated in the preparation of CCVs demonstrated that the final CCV fraction was significantly enriched for clathrin and CLASPs, including CLATHRIN HEAVY CHAINs (CHCs), CLATHRIN LIGHT CHAIN2 (CLC2), adaptor protein complex (AP1 and AP2) components, and the CLASP EPIDERMAL GROWTH FACTOR RECEPTOR PATHWAY SUBSTRATE INTERACTING PROTEIN (EPSIN1; i.e. EPN1; Lee et al., 2007) (Figure 7A). The presence of both AP1 and AP2 demonstrated that the final enriched CCV fraction includes TGN-derived and endocytic CCVs (Chen et al., 2011). The final enriched CCV fractions were also enriched in the CP and endosomal *trans*-soluble *N*-ethylmaleimide-sensitive factor attachment receptors (t-SNARES), KN, and SYNTAXIN OF PLANTS21 (SYP21), respectively, highlighting the enrichment of late secretory pathway membrane targeting and fusion proteins in clathrin-enriched fractions. By contrast, marker proteins for the endoplasmic reticulum (SEC12; Bar-Peled and Raikhel, 1997), *cis*-Golgi (MANNOSIDASE 1A/B [MAN1A/B]; Preuss et al., 2004), vacuole (VACUOLAR ATP SYNTHASE E1 [VHA-E1]; Strompen et al., 2005), chloroplast (TRANSLOCON AT THE OUTER ENVELOPE MEMBRANE OF CHLOROPLASTS33 [TOC33]; Ivanova et al., 2004), peroxisome

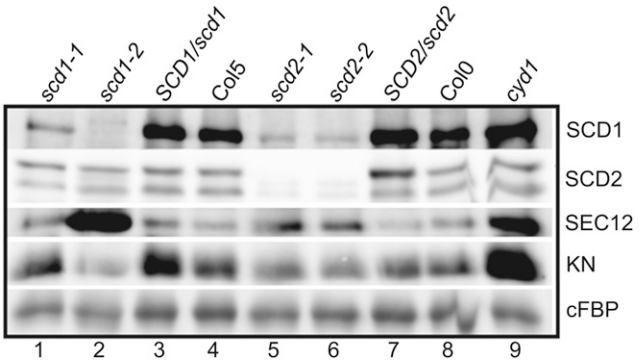

Figure 6. SCD1 Protein Levels Are Reduced in *scd1* and *scd2* Mutants.

Immunoblot analysis of SCD1 and SCD2 protein levels in total protein extracts (30 μg per lane) from the wild type (lanes 4 and 8), *scd1* (lanes 1 and 2), *scd2* (lanes 5 and 6), and *cyd1* (lane 9) mutants and rescued *scd* mutant lines (lanes 3 and 7) 10 DAG. Faint bands observed to comigrate with the SCD2 doublet in null *scd2* mutants (lanes 5 and 6) are likely the result of nonspecific interactions with anti-SCD2$^{N\text{-}term}$. Blots were probed for membrane-associated SEC12 and KN proteins and soluble cFBP protein as loading controls. See text for a discussion of the unequal SEC12 and KN protein levels observed between samples.

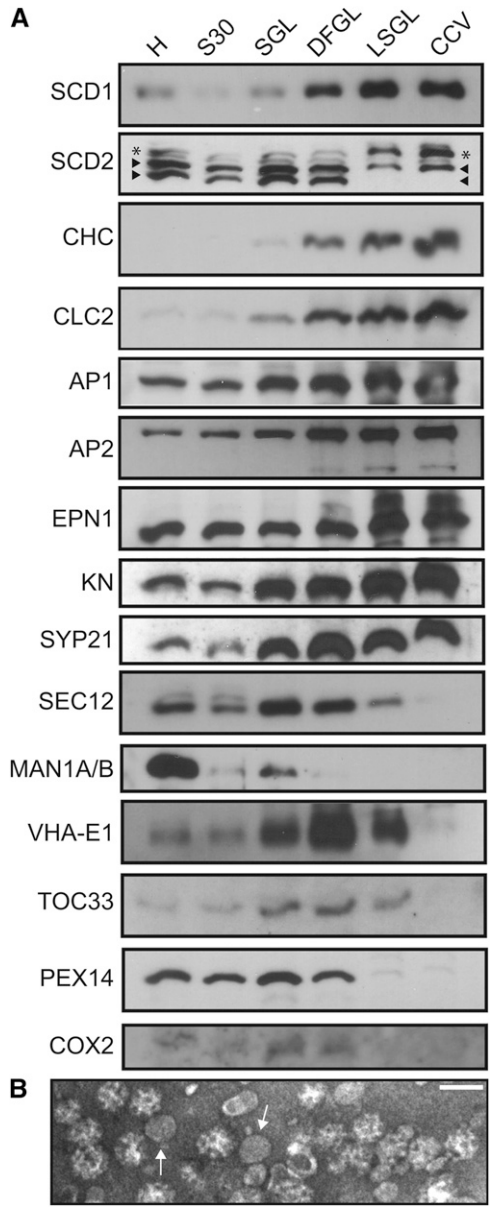

Figure 7. SCD1 and SCD2 Cofractionate with CCVs.

(A) Enriched CCVs were prepared from *Arabidopsis* T87W suspension-cultured cells, and equal amounts of protein from successive subcellular fractions generated during the CCV purification procedure were analyzed by immunoblotting with antibodies against SCD1, SCD2, structural components of the plant clathrin coat (CHC, CLC2, AP1, AP2, and EPN1), and various subcellular organelle marker proteins, including KN (CP), SYP21 (post-Golgi), SEC12 (endoplasmic reticulum), MAN1A/B (Golgi), VHA-E1 (tonoplast), TOC33 (chloroplast), PEX14 (peroxisome), and COX2 (mitochondria). Arrowheads and asterisk in the SCD2 panel indicate the SCD2 doublet (as in Figure 6) and a band of higher apparent molecular mass, respectively. The latter appears enriched in the final two fractions but is absent in immunoblots of whole-seedling extracts. H, homogenate; S30, 30,000*g* supernatant; SGL, Suc step gradient load; DFGL, linear deuterium oxide/Ficoll gradient load; LSGL, linear Suc gradient load; CCV, CCV fraction.
(B) Negative-stain TEM analysis of CCV-enriched fraction showing clathrin and noncoated membranes (arrows). Bar = 100 nm.

(PEROXIN14 [PEX14]; Hayashi et al., 2000), and mitochondria (CYTOCHROME OXIDASE2 [COX2]; Klodmann et al., 2011) were significantly depleted in the final CCV preparations (Figure 7A).

Importantly, immunoblot analysis using affinity-purified anti-SCD1^{DENN} and -SCD2$^{N\text{-}term}$ antibodies demonstrated that these two proteins cofractionated with CCVs (Figure 7A). Consistent with our immunoblot analysis of SCD2 protein in seedling total protein extracts (Figure 6), we detected two major ~64- and ~72-kD polypeptides in the *Arabidopsis* suspension-cultured cell homogenate (Figure 7A, arrowheads), as well as an additional polypeptide with higher apparent molecular mass of ~80 kD (Figure 7A, asterisk; see Supplemental Figure 7 online) that was below detection in whole-seedling extracts. Notably, the ~72- and ~80-kD polypeptides detected with the affinity-purified anti-SCD2$^{N\text{-}term}$ antibody were enriched (Figure 7A, asterisk and top arrowhead), whereas the ~64-kD polypeptide was depleted, in CCV-enriched fractions (Figure 7A, bottom arrowhead). Unlike KN, an integral membrane protein, SCD1 and the ~64-, ~72-, and ~80-kD SCD2 polypeptides were released from microsomal membranes after treatment with 6 M urea (see Supplemental Figure 7 and Supplemental Methods 4 online). Low but detectable levels of soluble SCD1 and the ~64- and ~72-kD SCD2 polypeptides were also present in membrane-free cytosol (S150) (see Supplemental Figure 7 online), indicating that SCD1 and SCD2 are peripheral membrane proteins.

To corroborate the presence of SCD1 and SCD2 on CCVs, we further characterized the CCV-enriched fraction via immunoelectron microscopy (see Supplemental Methods 5 online). The embedded CCV suspension was thin-sectioned (60 to 100 nm) to achieve a broad distribution of exposed epitopes (e.g., clathrin coat and membrane surface). Probing sections with the anti-CLC2 and -SCD1^{DENN} antibodies clearly demonstrated the presence of CLC2 and SCD1 on a subpopulation of vesicles (see Supplemental Figure 6 online). However, attempts to use the affinity-purified anti-SCD2$^{N\text{-}term}$ antibody to localize the SCD2 protein were unsuccessful, suggesting that the antibody is not suitable for immunoelectron microscopy analysis under the conditions used (see Supplemental Figure 6 online). Large-field views of sections probed with anti-CLC2, -SCD1^{DENN}, -SCD2$^{N\text{-}term}$, and the anti-rabbit:10-nm gold conjugate secondary antibodies (control) revealed a strong specificity and an apparently higher proportion of vesicles labeled with anti-CLC2 versus those with anti-SCD1^{DENN} (see Supplemental Figure 6 online). However, it is possible that this result reflects differences in epitope availability rather than reduced levels of SCD1 on a given vesicle relative to another.

Impaired Endocytosis in *scd1* and *scd2* Mutants

Based upon the cytokinesis and cell expansion defects of *scd1* and *scd2* mutants and their cofractionation with AP1 and AP2 CCVs, we hypothesized that SCD1 and SCD2 proteins are required for post-Golgi and/or endocytic trafficking. To determine whether PM endocytosis is impaired in the *scd* mutants, we used CLSM to monitor the cellular internalization of the lipophilic dye FM4-64 (http://www.lifetechnologies.com/order/catalog/product/T3166) in the roots of wild-type and *scd* seedlings (Figure 8). Representative images showed a decrease in the number of FM4-64–labeled fluorescent puncta within root cells of *scd1-1*, *scd1-2*, and

scd2-1 mutants after 10 min compared with wild-type cells (Figures 8A to 8D). Quantification of FM4-64 internalization, expressed as the average ratio of intracellular fluorescent signal per unit area versus that of PM, normalized to the wild type, revealed endocytosis was significantly reduced in *scd2-1*, *scd1-1*, and *scd1-2* compared with the wild type, respectively (Figure 8E).

Colocalization of SCD1 and SCD2 with Clathrin at the PM

Given that SCD1 and SCD2 cofractionate with CCVs, and that *scd1* and *scd2* mutants display impaired FM4-64 internalization, we examined whether N-terminally GFP-tagged SCD1 and/or SCD2 colocalize with CCPs at the cell cortex by variable-angle epifluorescence microscopy (VAEM; Konopka and Bednarek, 2008b). Expression of GFP-SCD1 and GFP-SCD2 under the control of their native promoters in homozygous *scd1-1* and *scd2-1*, respectively, rescued the phenotypic growth and developmental defects of *scd1-1* and *scd2-1* mutants (see Supplemental Figure 8 and Supplemental Methods 6 online), demonstrating that the GFP-tagged SCD1 and SCD2 fusion constructs are functional. Similar to CLC-mOrange, which localizes to CCPs (Konopka et al., 2008), VAEM imaging of epidermal root cells of seedlings expressing GFP-SCD1 or GFP-SCD2 revealed that these two proteins likewise localize at or near the PM in discrete dynamic foci (see Supplemental Figure 9 online). Intriguingly, in *GFP-SCD1/scd1-1* and *GFP-SCD2/scd2-1* lines coexpressing CLC2-mOrange, we observed a subpopulation of foci at or near the PM that contained both GFP-SCD1 and CLC2-mOrange or GFP-SCD2 and CLC2-mOrange (Figures 9C, 9F, 9I, and 9L). Colocalization of GFP-SCD1 and CLC2-mOrange or GFP-SCD2 and CLC2-mOrange was quantitatively verified using the Costes randomization test (Costes et al., 2004). Image pairs (Figures 9A and 9B, and 9G and 9H) were analyzed with 200 Costes iterations using a 0.432-μm (4-pixel) point spread function. The Pearson coefficients of both pairs were higher than that of all 200 iterations of each respective analysis, resulting in a Costes P value of 1.000 for both pairs. A P value greater than 0.95 is taken to demarcate colocalization, demonstrating that a subpopulation of SCD1 and SCD2 foci at or near the PM contain CLC2.

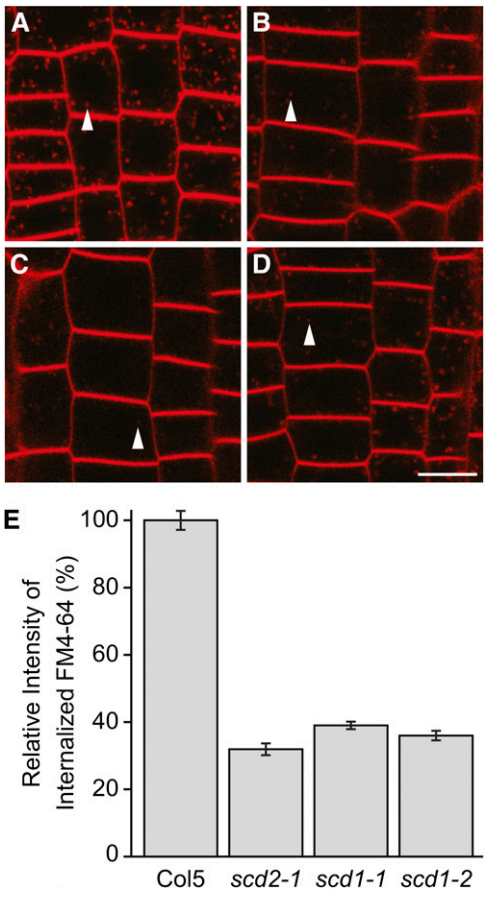

Figure 8. *scd1-1* and *scd2-1* Mutants Are Impaired in Endocytosis.

(A) to **(D)** Internalization of FM4-64 after 10 min in roots of the wild type (**[A]**; Col-5), *scd2-1* **(B)**, *scd1-1* **(C)**, and *scd1-2* **(D)**. Arrowheads indicate FM4-64–labeled vesicles. Bar = 10 μm.

(E) Mean relative intensity of internalized FM4-64. *n* = 18 to 21 fields per genotype ± SE.

DISCUSSION

scd Mutant Phenotypes

To further define and understand the molecular machinery of CP assembly and cell expansion, we identified and characterized *scd2* mutants that display phenotypic similarity to *scd1* mutants, including cytokinesis defects in stomata and epidermal pavement cells (Figures 1 to 3; Falbel et al., 2003). *scd2* and *scd1* mutants also show cell expansion defects; both mutants are dwarfs with short roots, are infertile, and display growth-related Suc hypersensitivity (Figures 2 and 5; see Supplemental Figure 3 online). The compressed root division and transition zone phenotype of *scd2* mutants suggests a possible defect in maintenance of auxin and/or cytokinin gradients in the roots of these mutants. This may result from, for example, perturbed polarization of PM auxin and/or cytokinin transporters perhaps due to misregulated endocytosis and/or recycling (Jung and McCouch, 2013). Experiments to determine the distribution of these hormones and transporters in *scd* mutants will be necessary to test this model.

A feature that we first detected in the epidermis of *scd2* mutant leaves is the presence of gaps and nearly symmetric arrangements of small cells. Subsequently, reanalysis of *scd1-2* leaves showed this to be a common feature of both *scd1* and *scd2* null mutants (see Supplemental Figures 1 and 2 online). Cell clusters of this type were observed in several stomatal patterning mutants, including the *speechless* (*spch*) cell fate transcription factor mutant (MacAlister et al., 2007; Pillitteri et al., 2007), the *mas/gsl8/chor* callose synthase mutant (Töller et al., 2008; Chen et al., 2009; Thiele et al., 2009; Guseman et al., 2010), and the *breaking of asymmetry in the stomatal lineage* (*basl*) stomatal asymmetric cell division control mutant (Dong et al., 2009), and are thus likely indicative of defects in signaling-dependent asymmetric epidermal leaf cell division in *scd1-2* and *scd2-1* mutants. The clusters of small cells and space/gaps observed in the leaf epidermis of *scd2-1* or both *scd2-1* and *scd1-2* mutants,

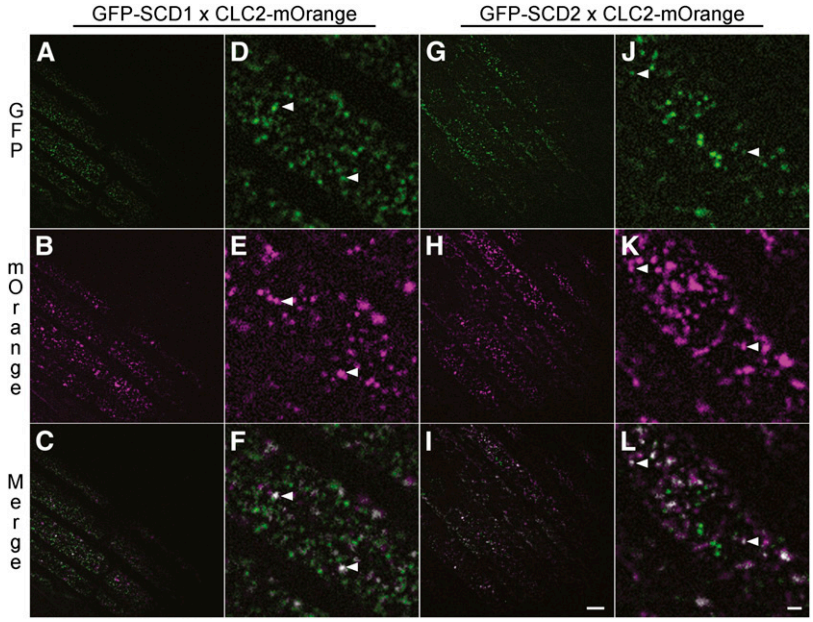

Figure 9. GFP-SCD1 and GFP-SCD2 Colocalize with CLC2-mOrange in Foci at or Near the PM.

Images of root epidermal cells expressing GFP-SCD1 and CLC2-mOrange (**[A]** to **[F]**) or GFP-SCD2 and CLC2-mOrange (**[G]** to **[L]**) as visualized by dual-channel VAEM of GFP (green; top panels), mOrange (magenta; center panels), and merged (bottom panels). **(D)** to **(F)** and **(J)** to **(L)** are higher magnification views of insets in **(A)** to **(C)** and **(G)** to **(I)**, respectively. Arrowheads denote representative foci at or near the PM that display colocalization of CLC2-mOrange and either GFP-SCD1 or GFP-SCD2. Bars = 5 μm in **(A)** to **(C)** and **(G)** to **(I)** and 1 μm in **(D)** to **(F)** and **(J)** to **(L)**.

respectively, suggest that SCD proteins play an important role in proper patterning of the leaf epidermis.

The spaces observed between *scd2* epidermal leaf cells appear to lack a PM (as shown by a lack of GFP-LTI6b signal) and stain strongly with PI (see Supplemental Figure 1 online), which binds to the pectin methylesterase–acidified pectins found in mature plant primary CWs (Rounds et al., 2011). These PI-staining spaces are also seen in *exocyst complex component84b* (*exo84b*) exocyst mutants, which, like *scd* mutants, manifest cytokinesis defects in stomata and display overall organ elongation defects (Fendrych et al., 2010). The exocyst is a heterooctomeric complex that functions to tether vesicles to their target membranes at the PM and developing CP to drive membrane fusion events (Thellmann et al., 2010; Fendrych et al., 2013) and has been shown in fission yeast to tether trafficking vesicles to actin filaments (Bendezú et al., 2012). In addition to the presence of spaces/gaps in the leaf epidermis, plant exocyst subunit mutants display a variety of cell expansion defects, including retarded hypocotyl elongation and tip-directed polar growth of pollen tubes, root hairs, and stigmatic papillae (Cole et al., 2005; Synek et al., 2006; Hála et al., 2008). The similarity of the cell expansion and cytokinesis defects of *scd1*, *scd2*, and exocyst mutants supports a role for the SCD proteins in endomembrane trafficking.

The clusters of small cells observed in the epidermis of *scd2-1* (see Supplemental Figure 2 online) are reminiscent of the overproliferation of small, stomatal lineage cells found in the leaf epidermis of *SPCH* overexpressors (MacAlister et al., 2007; Pillitteri et al., 2007) and loss-of-function *gsl8*/*chor* callose synthase mutants (Chen et al., 2009; Guseman et al., 2010). *gsl8*/*chor* plants also show stomatal cytokinesis defects, perhaps due to the reduction of callose in developing CPs of this mutant (Chen et al., 2009; Guseman et al., 2010). Loss of *CHOR* results in intercellular diffusion of the stomatal cell lineage initiation- and division-promoting transcription factor *SPCH*, presumably due to the loss of plasmodesmatal callose in *chor* (Guseman et al., 2010). Clusters of small cells are also characteristic of mutants lacking BASL, a protein of unknown function that dictates asymmetric cell division within the stomatal lineage (Dong et al., 2009). Analysis of the expression and localization of BASL, SPCH, and other GC fate markers as well as the generation of double *scd* stomatal lineage defective mutants will be necessary to confirm the identity of the small cells clustered in the *scd2-1* epidermis and the role of SCD1and SCD2 in stomatal patterning and asymmetric division.

Notably, *scd2* and *scd1* mutants display some phenotypic differences. *scd1* mutants lack mature trichomes since they expand abnormally and ultimately burst, while trichome development in *scd2* is unaffected. Similarly, *scd1* root hairs are shorter and are often branched and/or less regular along their length, indicating a defect in maintenance of focused polar cell expansion during root hair development, whereas *scd2* mutant root hairs appear normal (Falbel et al., 2003; see Supplemental Figure 3 online). Aside from these differences, the mutants displayed highly similar phenotypes, prompting investigation into the possible interaction of SCD2 and SCD1 through epistasis analysis and assessment of SCD1 protein abundance in *scd1* and *scd2* mutants. *scd1-2 scd2-1* double mutants are phenotypically indistinguishable from single *scd1-2* mutant lines (Figure 5). Furthermore, *scd2*

mutants show significant reduction in SCD1 protein levels, whereas SCD2 levels are unaffected in *scd1* mutants (Figure 6). Together, these data indicate that SCD1 and SCD2 operate in a common pathway and, moreover, that SCD1 function requires SCD2. Although *scd1* and *scd2* mutants share many similar defects, their phenotypic differences suggest that SCD1 and SCD2 may also have independent functions. Alternatively, the phenotypic differences may be due to the residual low levels of SCD1 in *scd2* mutants and/or partial redundancy of the other members of the SCD2 protein family with SCD2.

SCD Proteins Are Potential Membrane Trafficking Regulators

SCD2 is a member of a small plant-specific gene family whose members are predicted to encode proteins that share a common domain of unknown function (the SCD2 domain) and at least one central coiled-coil domain (see Supplemental Table 1 and Supplemental Figure 4 online). Coiled-coil domains are one of the most highly abundant interacting motifs represented in eukaryotic proteomes and mediate diverse cellular functions such as transcription, signaling, and protein folding (Wang et al., 2012); thus, their presence does not suggest any specific function. The SCD1 protein contains a DENN domain (Falbel et al., 2003), which has been shown biochemically to have specific Rab GEF activity in all 17 members of the human DENN domain protein family (Yoshimura et al., 2010; Marat et al., 2011), defining the DENN domain as a characteristic of vesicle trafficking regulators. The DENN domain–containing Rab GEFs connecdenn 1, 2, and 3 have also been shown to bind clathrin and the clathrin adaptor AP2 (Marat and McPherson, 2010), and connecdenn 3 has recently been shown to bind actin (Marat et al., 2012), linking activation of Rab35 with clathrin and cytoskeletal dynamics. Rab35 mediates late secretory pathway vesicle trafficking (i.e., PM to endosome and vice versa) (Patino-Lopez et al., 2008; Sato et al., 2008) and is necessary for the late stages of animal cytokinesis, which involves both anterograde and retrograde vesicle trafficking (Kouranti et al., 2006) reminiscent of the vesicular trafficking required for CP assembly in plant cells. No Rab35 homologs have been discovered in plants, yet plants have a widely expanded Rab11 family (Rutherford and Moore, 2002), one or more of whose members likely serve the function of Rab35 in plants. The cell expansion and cytokinesis defects of *scd1* and *scd2* mutants implicate SCD1 and SCD2 in Golgi to PM and/or CP vesicle trafficking through regulation of a late secretory pathway, with SCD1 in particular likely functioning as a Rab GEF. Consistent with this, cytokinesis-defective *scd1-2* leaf cells accumulate unfused secretory vesicles (Falbel et al., 2003), a hallmark of defects in Rab and/or Rab GEF function (Novick et al., 1980, 1981).

SCD Proteins Participate in Clathrin-Mediated Trafficking

Using subcellular fractionation and live-cell imaging, we demonstrated that SCD1 and SCD2 are associated with isolated CCVs and colocalized with CLC2 in dynamic CCPs at or near the PM (Figure 9; see Supplemental Figure 9 online). Additionally, *scd1* and *scd2* mutants displayed defects in the internalization of FM4-64 from the PM (Figure 8), which has previously been demonstrated to be in part dependent upon CME (Dhonukshe et al., 2007; Wang et al., 2013). Together, these data strongly support our hypothesis that SCD1 and SCD2 participate in clathrin-mediated trafficking events at the PM. However, it cannot be ruled out that the SCD proteins participate in other endomembrane pathways nor that the inhibition of SCD1 and SCD2 function at other stages of the late secretory pathway may indirectly affect the uptake of FM4-64. Further experiments are necessary to determine the subcellular localization and role of SCD1 and SCD2 in trafficking of bona fide cargo proteins to and from the TGN and PM.

CCV trafficking of proteins, including vacuolar proteins from the TGN and endocytic compartments, as well as internalized PM proteins via CME are essential for plant growth, development, and signaling (Song et al., 2006; Dhonukshe et al., 2007; Robert et al., 2010; Kitakura et al., 2011; Adam et al., 2012; Wang et al., 2013). In mammalian cells, CME and the formation of CCVs at the TGN involve the coordinated interplay of accessory and regulatory proteins that is initiated by binding of the cargo AP complexes and their recruitment of clathrin triskelia. To date, at least four AP complexes (AP1 to AP4) have been identified to be encoded by the genomes of animals and plants, and in mammalian cells, localization and functional studies have demonstrated that AP2 and AP1 mediate the formation of CCVs at the PM and TGN, respectively. In addition to their role in binding cargo and clathrin, AP complexes also interact with accessory proteins (i.e., CLASPs) required for the formation and subsequent trafficking of CCVs.

Like the animal CLASP connecdenn 1, which is postulated to be recruited to budding CCVs via its C-terminal interactions with AP2 (Allaire et al., 2006, 2010), SCD1 was found to coimmunoprecipitate with the μ-subunit of AP2 (Yamaoka et al., 2013). However, unlike connecdenn 1, which harbors the well-defined Phe-X-Asp-X-Phe (FxDxF), where x is any amino acid, and Trp-X-X-Phe-acidic (WxxF-acidic) AP2 α-subunit binding motifs (Allaire et al., 2006), SCD1 and SCD2 lack these interaction motifs. However, SCD1 and SCD2 do contain Tyr- or dileucine-based motifs (i.e., Tyr-X-X-hydrophobic and bulky [YxxΦ] and Glu/Asp-X-X-X-Leu-Leu/Ile [(E/D)xxxL(L/I)]) (see Supplemental Figure 5 online) that in animals and yeast mediate the interaction of connecdenn 1 to 3 and other proteins with the μ-subunits of AP1, AP2, and AP3 (Bonifacino and Traub, 2003). SCD proteins may also bind clathrin directly as both SCD1 and SCD2 contain several potential type I clathrin box motifs (Leu-bulky and hydrophobic-polar-bulky and hyrophobic-Asp/Glu [LΦpΦ(D/E)]; Dell'Angelica, 2001) (see Supplemental Figure 5 online). Interestingly, AP2-interacting Tyr-based, dileucine-based, and α-subunit binding Asp-X-Phe (DxF) motifs as well as the Asn-X-X-Tyr (NxxY) motif, which is required for Rab21-mediated CME of integrins and cytokinesis (Pellinen et al., 2008), are present in the primary sequence of the putative *Arabidopsis* SCD2-related proteins (see Supplemental Figure 5 online), suggesting that other members of the SCD2 protein family may similarly function in CCV trafficking.

SCD2 Function and Regulation

Immunoblot analysis of whole-seedling total protein extracts (Figure 6) and enriched CCV fractions (Figure 7) using affinity-purified anti-SCD2$^{N\text{-}term}$ antibodies revealed the presence of several discrete polypeptides of increasing molecular mass that were

absent in *scd2* loss-of-function mutants. Notably, we reproducibly observed a significant reduction in the level of the 64-kD SCD2 polypeptide, which is the predicted molecular mass of the full-length SCD2 protein, with a concomitant increase in the amounts of the ~72- and ~80-kD SCD2 isoforms in enriched CCVs relative to the total soluble and membrane cell lysate (Figure 7, CCV versus H samples). Our current working hypothesis is that the CCV-associated SCD2 ~72- and ~80-kD isoforms are the result of monoubiquitination (8 kD) and diubiquitination (16 kD) of 64-kD SCD2. Indeed, polyubiquitination is critical for the clathrin-mediated recycling of PM proteins in yeast, mammals, and plants, including the *Arabidopsis* PIN-FORMED2 auxin efflux carrier (Szymkiewicz et al., 2004; Leitner et al., 2012). Intriguingly, two DDB1-binding WD-40 (DWD) motifs were identified within the WD-40 repeats of SCD1, suggesting it could function as a substrate receptor for a CULLIN4-based oligomeric E3 ubiquitin ligase (Lee et al., 2008), possibly targeting SCD1 and SCD2 for subsequent recruitment by the clathrin vesicle coat machinery during endocytosis (Szymkiewicz et al., 2004).

The cytokinesis and cell expansion defects displayed by *scd1* and *scd2* mutants, together with the SCD1 DENN domain structure that suggests a membrane transport or cytoskeletal assembly regulatory function, the intimate interplay between *SCD1* and *SCD2* expression, and, perhaps most telling, the cofractionation and colocalization of SCD1 and SCD2 proteins with the clathrin machinery strongly suggest a role for the SCD proteins together in membrane trafficking events critical to cytokinesis and cell expansion. Future investigation is necessary to define which particular membrane trafficking pathway(s) involves one or both SCD proteins. It is interesting to note that the cytokinesis defects observed in the *scd* mutants occur primarily in GMCs and are not observed in, for example, root cells (Falbel et al., 2003; Figure 2). GMC formation is dependent upon a sequence of numerous asymmetric divisions, with the final symmetric division of the GMC yielding the two GCs that surround the pore of the stomatal complex. Little is known about the role of membrane trafficking during cytokinesis of asymmetrically dividing cells. Perhaps cytokinesis at the division symmetry transition of stomatal lineage cells is particularly susceptible to the loss of SCD-dependent membrane trafficking in the *scd* mutants. It will be interesting to investigate how the SCD proteins link regulation of membrane trafficking to cytoskeletal regulation, and further, to intra- and intercellular signaling events that regulate cell division symmetry, and, hence, stomatal patterning.

METHODS

Plant Materials and Growth Conditions

Arabidopsis thaliana seed sources are as follows: fast-neutron mutants (M1G-01A-02; Lehle Seeds); Col-5 wild-type (CS28175), 29-1 (CS84726; Cutler et al., 2000), and N7 (CS84731; Cutler et al., 2000; ABRC); T-DNA insertion mutant *scd2-2* (GK_129C05; GABI-Kat) (Li et al., 2007); CLC2-mOrange transgenic lines as previously described (Konopka et al., 2008); and *scd1* and $KAT1_{pro}$*-GUS* (Nakamura et al., 1995) as previously described (Falbel et al., 2003). Heterozygous *scd2-1* lines were backcrossed three times to Col-5 (i.e., Col-0 *gl*-1) prior to characterization. Seeds were sterilized for 5 and 1 min in 70% (v/v) ethanol, 0.1% (v/v) Triton X-10, and 95% (v/v) ethanol, plated on solid germination medium (half-strength MS [Murashige and Skoog, 1962] and 0.6 or 1% [w/v] agar) containing indicated antibiotics or sugars, stratified for 3 d at 4°C, and then grown under continuous light at 22°C. Soil-grown plants were germinated on or transferred to Metro-Mix360 (SunGro Horticulture) and grown under long days (16 h light/8 h dark) at 17 or 22°C. Whole seedlings and plants were imaged using a Nikon CoolPix digital camera (Nikon Instruments). *Arabidopsis* T87W cells (Axelos et al., 1992) were grown on a gyrorotatory shaker (140 rpm) in MS, 0.2 mg/L 2,4-D, and 1.32 mM KH_2PO_4 under continuous light at 22°C and subcultured into fresh media (1:10 dilution) weekly.

Plasmid Construction and Generation of Transgenic Plants

All PCR-generated cloning fragments used in these studies (see Supplemental Table 3 online) were produced using Phusion DNA polymerase (F-530; Thermo Fisher Scientific), and all oligonucleotide primers (see Supplemental Table 4 online) were synthesized by Integrated DNA Technologies. Transgenic plants were generated via *Agrobacterium tumefaciens*–mediated floral dip (Clough and Bent, 1998).

For *scd2-1* rescue, heterozygous *scd2-1* plants transformed with $SCD2_{pro}$*-SCD2* (see Supplemental Table 3 online) were selected on one-half-strength MS and 50 mg/L kanamycin (Kan), and T2 and T3 plants confirmed to be homozygous for *scd2-1* (*SCD2*/*scd2-1*) were used for analysis. Kan-resistant T2 and T3 plants from a transformation of Col-2 with $SCD2_{pro}$*-GUS* (see Supplemental Table 3 online) were used for *SCD2* spatial expression analysis. $SCD1_{pro}$*-GFP-SCD1* was transformed into homozygous *scd1-1* plants grown at the permissive temperature, and transgenic *GFP-SCD1*/*scd1-1* plants were selected on one-half-strength MS and 50 mg/L of Kan. *GFP-SCD2*/*scd2-1* was transformed into heterozygous *scd2-1* plants, and transgenic *GFP-SCD2*/*scd2-1* plants were selected as for *GFP-SCD1*/*scd1-1* above.

Double Mutant Analysis

Heterozygous *scd1-2 scd2-1* F2 plants were grown vertically on one-half-strength MS and 1% (w/v) Suc and scanned on a flatbed scanner (CanoScan N24OU; Canon) at 3- to 7-d intervals. Seedlings were transferred to fresh media 25 DAG. Roots were measured using ImageJ software (Schneider et al., 2012). Seedlings were collected for PCR genotyping analysis at 48 DAG or when their roots reached the bottom of the culture plate.

Histochemistry and Light Microscopy

TBO-stained epidermal peels were prepared as previously described (Falbel et al., 2003) and imaged using a Zeiss Axioskop (Carl Zeiss Microscopy) with a Leica DFS480 digital camera using Leica FireCam software (Leica Microsystems). F2 plants from *scd2-1* crosses to 29-1 (i.e., GFP-LTI6b) and N7 (Cutler et al., 2000) lines were germinated on half-strength MS and 15 mg/L of glyphosate and imaged via CLSM (Nikon C1; Nikon Instruments) using ×60 or ×100 oil immersion objectives (numerical aperture = 1.4 for both). To visualize CWs, plants were stained with PI as previously described (Falbel et al., 2003) and imaged via CLSM as above. CLSM images were false colored, merged, and/or adjusted for brightness and contrast using Adobe Photoshop CS5 (Adobe Systems). Cotyledon pavement cell area was calculated using ImageJ software (Schneider et al., 2012).

F2 plants of *scd2-1* × $KAT1_{pro}$*-GUS* crosses (Nakamura et al., 1995) or Col2:$SCD2_{pro}$*-GUS* T2 plants were germinated on half-strength MS and 50 mg/L of Kan and processed as follows: Tissue was fixed in ice-cold 90% (v/v) acetone (10 to 15 min on ice), rinsed two times (50 mM $NaPO_4$, pH 7.0), vacuum infiltrated four to six times with GUS staining solution (0.5 mM 5-bromo-4-chloro-3-indoyl-β-D-glucuronide, 0.5 mM $K_3[Fe(CN)_6]$, 0.5 mM $K_4[Fe(CN)_6]$, 0.5% [v/v] Triton X-100, and 50 mM $NaPO_4$, pH 7.0), and incubated at 37°C overnight, and phytopigments were removed via several

changes of 70% (v/v) ethanol at 37°C. Images were obtained using Leica MZ6, Leica M165FC, or Zeiss Axioskop microscopes as above. Whole seedlings were mounted on 1% (w/v) agar to which white paint was added until the desired opacity was achieved and imaged using a Nikon CoolPix digital camera (Nikon Instruments). Analysis of internalization of the lipophilic dye FM4-64 (2 μM) was performed as previously described (Wang et al., 2013). Data were collected from three independent experiments measuring 30 individual roots, 10 to 15 cells per root. A Student's *t* test (paired with two-tailed distribution) was used for statistical analysis.

For VAEM, *GFP-SCD1/scd1-1* and *GFP-SCD2/scd2-1* T2 plants were crossed to CLC2-mOrange (Konopka et al., 2008), and F3 plants of *GFP-SCD1/scd1-1* or *GFP-SCD2/scd2-1* × CLC2-mOrange were germinated on half-strength MS, 50 mg/L of Kan, and 15 mg/L of glyphosate. Nine DAG, segregating seedlings were transferred to media without selection and allowed to recover for 6 d prior to imaging. The epidermal cells of representative seedling roots of each genotype ($n > 5$) were then observed by VAEM on a Nikon EclipseTE2000-U inverted microscope equipped with a ×100, 1.45–numerical aperture Plan Apo total internal reflection fluorescence microscopy objective using 488-nm argon and 543-nm HeNe lasers (Melles Griot). Images of GFP and mOrange channels were acquired sequentially as averages of four 500-ms exposures with an Evolve 512 EMCCD camera (Photometrics). Images were processed using the ImageJ (Schneider et al., 2012) rolling ball background subtraction tool (0.540-μm ball radius) and subsequently analyzed using the Colocalization Threshold and Coloc2 plug-ins, which employ the Costes image randomization test as described (Costes et al., 2004).

Immunoblot Analysis

Liquid N_2-ground seedlings or N_2 decompression-lysed cultured cells (using a 45-mL Parr cell disruption vessel; Parr Instrument Company) were solubilized in Laemmli sample buffer (Laemmli, 1970), and protein concentrations were determined using 660-nm protein assay reagent containing ionic detergent compatibility reagent (22660 and 22663; Thermo Fisher Scientific) according to the manufacturer's instructions using BSA as a standard. Equal total protein was resolved using SDS-PAGE and transferred to nitrocellulose by electroblotting (2 h at 300 mA). After blocking in PBS-T (2.7 mM KCl, 137 mM NaCl, 1.9 mM KH_2PO_4, 10 mM Na_2HPO_4, and 0.1% [v/v] Tween 20, pH 7) and 5% (w/v) milk (30 to 60 min at 22°C or overnight at 4°C), blots were incubated with primary antibody in the above PBS-T milk blocking buffer (several hours to overnight at 4°C with gentle shaking). Affinity-purified antibodies were generated as previously described: anti-SCD1^{DENN} (Korasick et al., 2010), anti-CLC2 (Wang et al., 2013), anti-KN (Rancour et al., 2002), anti-MAN1A/B (Preuss et al., 2004), anti-RGP1 (Delgado et al., 1998), anti-SEC12 (Bar-Peled and Raikhel, 1997), anti-SYP21 (da Silva Conceição et al., 1997), and anti-TOC33 (Ivanova et al., 2004). Anti-CHC (sc-57684) was purchased from Santa Cruz Biotechnology. Anti-COX2 (AS04 053A), anti-VHA-E1 (AS07 213), anti-PEX14 (AS08 372), and anti-cFBP (AS04 043) were purchased from Agrisera. Anti-EPN1 (Lee et al., 2007), anti-AP2α, and anti-AP1γ were a gift from I. Hwang (Postech University, Pohang, Korea). After four washes in PBS-T, the blot was incubated with horseradish peroxidase–conjugated secondary antibodies (donkey anti-rabbit IgG or sheep anti-mouse IgG [NA934V or NA931V; Amersham Life Sciences]) in blocking buffer (1 h at 22°C). Blots were washed as above and then incubated in Lumi-Light or Lumi-Light^{PLUS} chemiluminescent substrate (12015200001 or 12015196001; Roche Applied Science) for 5 min at 22°C and exposed to film (BX810; MIDSCI) or imaged using an ImageQuant LAS4010 digital imaging system (GE Healthcare Life Sciences). Film exposures were digitized using a CanoScan N24OU scanner. Images were adjusted for contrast and brightness using Adobe Photoshop CS5.

Generation and Purification of Anti-SCD2$^{N\text{-}term}$ Antibodies

His_8-Maltose Binding Protein (MBP)-Tobacco Etch Virus protease recognition site (TEV)-SCD2$^{N\text{-}term}$ (see Supplemental Table 3 online) was expressed in *Escherichia coli* B834 pRARE2 (Blommel and Fox, 2007) from pVP16-TEV-SCD2$^{N\text{-}term}$ (see Supplemental Table 3 online) as follows: 1 liter of Luria-Bertani (Bertani, 1951), 50 mg/L of carbenicillin, and 34 mg/L of chloramphenicol were inoculated with a 50-mL saturated overnight culture, grown to $OD_{600} \approx 0.6$ (at 20°C), and induced with 0.5 mM isopropyl β-D-1-thiogalactopyranoside (2 h at 20°C). His_8-MBP-TEV-SCD2$^{N\text{-}term}$ was purified sequentially by affinity chromatography using amylose resin (E8021; New England Biolabs) followed by nickel-nitrilotriacetic acid (30210; Qiagen) according to the manufacturer's instructions, dialyzed against PBS, and its concentration determined by Bradford assay (500-0006; Bio-Rad) and SDS-PAGE followed by Coomassie Brilliant Blue staining and scanning densitometry using BSA as a standard. Rabbit antibodies were raised against His_8-MBP-TEV-SCD2$^{N\text{-}term}$ (Covance Research Products) and depleted of anti-His_8-MBP antibodies using immobilized His_8-MBP resin (Affi-Gel 10; Bio-Rad) prior to affinity purification of anti-SCD2$^{N\text{-}term}$ antibodies using immobilized His_8-MBP-TEV-SCD2$^{N\text{-}term}$ as described previously (Kang et al., 2001).

CCV Enrichment

Three to four days after subculturing, 60 to 90 mL of packed cell volume of T87W cells (Axelos et al., 1992) was harvested by centrifugation (4 min at 100*g*) and washed and resuspended in clathrin isolation buffer (1× CIB: 100 mM MES, 3 mM EDTA, 1 mM EGTA, and 0.5 mM $MgCl_2$) with protease inhibitors (1× protease inhibitor cocktail-DMSO-soluble and 1× protease inhibitor cocktail-water-soluble [Aris and Blobel, 1991], 1 mM DTT, and 10 μg/mL of E64). Cells were lysed by N_2 decompression (20 min at 1500 p.s.i. N_2) and centrifuged (4 min at 100*g*). CCVs were purified by differential and density gradient centrifugation essentially as described (Depta and Robinson, 1986; Harley and Beevers, 1989). Briefly, the cell homogenate (H) underwent sequential differential centrifugation (4 min at 100*g*, 10 min at 1000*g*, and 25 min at 30,000*g*). Microsomal membranes (Suc step gradient load) from the 30,000*g* supernatant (S30) were collected by centrifugation (60 min at 120,000*g*), resuspended in 1× CIB, layered onto a 10/40/50% (w/v) Suc step gradient, centrifuged (50 min at 116,000*g*), and fractions corresponding to the 10% and 10/40% Suc steps were harvested and centrifuged (50 min at 180,000*g*). The pellet was resuspended in 1× CIB (deuterium oxide/Ficoll gradient load), layered over a linear 90/2% to 90/30% (w/v) deuterium oxide/Ficoll gradient and centrifuged (12 to 14 h at 80,000*g*). Fractions containing enriched CCVs (equivalent to ~14 to 16% [w/w] Suc) were harvested and centrifuged (50 min at 264,000*g*), resuspended, applied to a 10 to 25% (w/v) linear Suc gradient, and centrifuged (1.5 h at 103,000*g*). Linear Suc gradient fractions (13 to 17% [w/w] Suc) were pooled and centrifuged (50 min at 264,000*g*) to yield the final enriched CCV fraction (typical yield: 100 to 300 μg). Note that all steps were performed at 0 to 4°C.

Negative-Stain EM

A thin layer of CCVs in 2% (w/v) OsO_4 was dried onto the surface of a Pioloform-coated 200 mesh Ni grid. Nano-W methylamine tungstate (Nanoprobes) was deposited over the sample and the excess removed with filter paper. Imaging was performed on a Philips CM120 transmission electron microscope (FEI/Philips Electron Optics) and a MegaViewIII side-mounted digital camera (Olympus) at the University of Wisconsin-Madison Medical School EM Facility. Quantitative analysis of CCVs versus uncoated vesicles was performed on randomly selected EM images of negative-stained samples using the ImageJ Cell Counter plug-in (http://rsb.info.nih.gov/ij/). Coated vesicles represented, on average, 76% ± 10% ($n = 11$) of the total vesicles counted.

Accession Numbers

Sequence data from this article can be found in the GenBank/EMBL data libraries under accession numbers AY082605 (SCD1 [At1g49040]), KC533769 (SCD2 [At3g48860]), AY113850 (At5g13260), AY735650 (At4g25070), AED93200 (At5g23700), and AEE82665 (At4g08630).

Supplemental Data

The following materials are available in the online version of this article.

Supplemental Figure 1. *scd* Leaf Epidermal Spaces.

Supplemental Figure 2. *scd* Leaf Epidermal Division Symmetry Defects.

Supplemental Figure 3. Suc-Sensitive *scd2* Phenotypes.

Supplemental Figure 4. Mapping and Cloning the *SCD2* Gene.

Supplemental Figure 5. Alignment of the Predicted Amino Acid Sequences of Members of the SCD2 Protein Family.

Supplemental Figure 6. CLC2 and SCD1 Are Detected on Isolated Clathrin-Coated Vesicles.

Supplemental Figure 7. SCD1 and SCD2 Are Peripheral Membrane Proteins.

Supplemental Figure 8. *GFP-SCD1* and *GFP-SCD2* Rescue of *scd1* and *scd2* Mutants.

Supplemental Figure 9. Time Lapse of CLC-mOrange, GFP-SCD1, and GFP-SCD2 Foci at or Near the Plasma Membrane.

Supplemental Table 1. The Lengths of SCD2 and Its *Arabidopsis* Homologs, and the Positions of Protein Domains within Each.

Supplemental Table 2. The Degree of Protein Sequence Identity and Similarity of the Four Predicted *Arabidopsis* SCD2 Homologs Compared Pairwise to SCD2.

Supplemental Table 3. Constructs Used in This Study.

Supplemental Table 4. Oligonucleotide Primers Used in This Study.

Supplemental Methods 1. Positional Cloning of *SCD2*.

Supplemental Methods 2. *scd2-1* dCAPS Analysis.

Supplemental Methods 3. Protein Sequence Analysis.

Supplemental Methods 4. Analysis of SCD1 and SCD2 Membrane Association.

Supplemental Methods 5. Immuno-EM.

Supplemental Methods 6. Genetic Rescue by *GFP-SCD* Transgenes.

ACKNOWLEDGMENTS

We thank Tom Martin and Michelle Kielar-Grevstad (University of Wisconsin-Madison) for CLSM/total internal reflection fluorescence microscopy use and instruction, Nou Vang (University of Wisconsin-Madison) and Easton Bednarek (Hamilton Middle School, Madison, WI) for help with CCV isolation, Inhwan Hwang (Postech University, Korea) for kindly providing antibodies, Ben August (University of Wisconsin-Madison Medical School EM Facility) for help in transmission electron microscope use and sample preparation, Tanya Falbel and Allison Doak (University of Wisconsin-Madison) for technical assistance, and Patrick Masson (University of Wisconsin-Madison) for critical reading and discussion of this article. This research was supported by funding from the U.S. National Science Foundation (1121998) and a Vilas Associate Award (University of Wisconsin-Madison) (S.Y.B.), by the Canadian National Sciences and Engineering Research Council (22R92904) (F.D.S.), and by the National Science Foundation of China (31370313 and 91317304) (J.P.).

AUTHOR CONTRIBUTIONS

C.M.M., G.D.R., L.M.K., C.W., N.J., J.N., M.B.G., and S.Y.B. performed research. C.M.M., G.D.R., L.M.K., C.W., N.J., J.P., F.D.S., and S.Y.B. analyzed data. F.D.S., J.P., and S.Y.B. directed research design. C.M.M., G.D.R., and S.Y.B. wrote the article.

Received June 20, 2013; revised September 17, 2013; accepted September 27, 2013; published October 25, 2013.

REFERENCES

Adam, T., Bouhidel, K., Der, C., Robert, F., Najid, A., Simon-Plas, F., and Leborgne-Castel, N. (2012). Constitutive expression of clathrin hub hinders elicitor-induced clathrin-mediated endocytosis and defense gene expression in plant cells. FEBS Lett. **586:** 3293–3298.

Allaire, P.D., Marat, A.L., Dall'Armi, C., Di Paolo, G., McPherson, P.S., and Ritter, B. (2010). The Connecdenn DENN domain: A GEF for Rab35 mediating cargo-specific exit from early endosomes. Mol. Cell **37:** 370–382.

Allaire, P.D., Ritter, B., Thomas, S., Burman, J.L., Denisov, A.Y., Legendre-Guillemin, V., Harper, S.Q., Davidson, B.L., Gehring, K., and McPherson, P.S. (2006). Connecdenn, a novel DENN domain-containing protein of neuronal clathrin-coated vesicles functioning in synaptic vesicle endocytosis. J. Neurosci. **26:** 13202–13212.

Aris, J.P., and Blobel, G. (1991). Isolation of yeast nuclei. Methods Enzymol. **194:** 735–49.

Axelos, M., Curie, C., Mazzolini, L., Bardet, C., and Lescure, B. (1992). A protocol for transient gene expression in *Arabidopsis thaliana* protoplasts isolated from cell suspension cultures. Plant Physiol. Biochem. **30:** 123–128.

Backues, S.K., Konopka, C.A., McMichael, C.M., and Bednarek, S.Y. (2007). Bridging the divide between cytokinesis and cell expansion. Curr. Opin. Plant Biol. **10:** 607–615.

Bar-Peled, M., and Raikhel, N.V. (1997). Characterization of AtSEC12 and AtSAR1. Proteins likely involved in endoplasmic reticulum and Golgi transport. Plant Physiol. **114:** 315–324.

Bashline, L., Li, S., Anderson, C.T., Lei, L., and Gu, Y. (2013). The endocytosis of cellulose synthase in Arabidopsis is dependent on μ2, a clathrin mediated endocytosis adaptin. Plant Physiol. **163:** 150–160.

Bendezú, F.O., Vincenzetti, V., and Martin, S.G. (2012). Fission yeast Sec3 and Exo70 are transported on actin cables and localize the exocyst complex to cell poles. PLoS ONE **7:** e40248.

Bertani, G. (1951). Studies on lysogenesis. I. The mode of phage liberation by lysogenic Escherichia coli. J. Bacteriol. **62:** 293–300.

Blommel, P.G., and Fox, B.G. (2007). A combined approach to improving large-scale production of tobacco etch virus protease. Protein Expr. Purif. **55:** 53–68.

Bonifacino, J.S., and Traub, L.M. (2003). Signals for sorting of transmembrane proteins to endosomes and lysosomes. Annu. Rev. Biochem. **72:** 395–447.

Chen, X., Irani, N.G., and Friml, J. (2011). Clathrin-mediated endocytosis: The gateway into plant cells. Curr. Opin. Plant Biol. **14:** 674–682.

Chen, X.-Y., Liu, L., Lee, E., Han, X., Rim, Y., Chu, H., Kim, S.-W., Sack, F.D., and Kim, J.-Y. (2009). The Arabidopsis callose synthase gene GSL8 is required for cytokinesis and cell patterning. Plant Physiol. **150:** 105–113.

Cheung, A.Y., Niroomand, S., Zou, Y., and Wu, H.-M. (2010). A transmembrane formin nucleates subapical actin assembly and

controls tip-focused growth in pollen tubes. Proc. Natl. Acad. Sci. USA **107:** 16390–16395.

Chow, C.-M., Neto, H., Foucart, C., and Moore, I. (2008). Rab-A2 and Rab-A3 GTPases define a trans-Golgi endosomal membrane domain in *Arabidopsis* that contributes substantially to the cell plate. Plant Cell **20:** 101–123.

Clough, S.J., and Bent, A.F. (1998). Floral dip: A simplified method for Agrobacterium-mediated transformation of *Arabidopsis thaliana*. Plant J. **16:** 735–743.

Cole, R.A., Synek, L., Žárský, V., and Fowler, J.E. (2005). SEC8, a subunit of the putative Arabidopsis exocyst complex, facilitates pollen germination and competitive pollen tube growth. Plant Physiol. **138:** 2005–2018.

Collings, D.A., Gebbie, L.K., Howles, P.A., Hurley, U.A., Birch, R.J., Cork, A.H., Hocart, C.H., Arioli, T., and Williamson, R.E. (2008). *Arabidopsis* dynamin-like protein DRP1A: A null mutant with widespread defects in endocytosis, cellulose synthesis, cytokinesis, and cell expansion. J. Exp. Bot. **59:** 361–376.

Costes, S.V., Daelemans, D., Cho, E.H., Dobbin, Z., Pavlakis, G., and Lockett, S. (2004). Automatic and quantitative measurement of protein-protein colocalization in live cells. Biophys. J. **86:** 3993–4003.

Cutler, S.R., Ehrhardt, D.W., Griffitts, J.S., and Somerville, C.R. (2000). Random GFP:cDNA fusions enable visualization of subcellular structures in cells of *Arabidopsis* at a high frequency. Proc. Natl. Acad. Sci. USA **97:** 3718–3723.

da Silva Conceição, A., Marty-Mazars, D., Bassham, D.C., Sanderfoot, A.A., Marty, F., and Raikhel, N.V. (1997). The syntaxin homolog AtPEP12p resides on a late post-Golgi compartment in plants. Plant Cell **9:** 571–582.

Deeks, M.J., Cvrcková, F., Machesky, L.M., Mikitová, V., Ketelaar, T., Zársky, V., Davies, B., and Hussey, P.J. (2005). *Arabidopsis* group Ie formins localize to specific cell membrane domains, interact with actin-binding proteins and cause defects in cell expansion upon aberrant expression. New Phytol. **168:** 529–540.

de Graaf, B.H.J., Cheung, A.Y., Andreyeva, T., Levasseur, K., Kieliszewski, M., and Wu, H.M. (2005). Rab11 GTPase-regulated membrane trafficking is crucial for tip-focused pollen tube growth in tobacco. Plant Cell **17:** 2564–2579.

Delgado, I.J., Wang, Z., de Rocher, A., Keegstra, K., and Raikhel, N.V. (1998). Cloning and characterization of AtRGP1. A reversibly autoglycosylated Arabidopsis protein implicated in cell wall biosynthesis. Plant Physiol. **116:** 1339–1350.

Dell'Angelica, E.C. (2001). Clathrin-binding proteins: Got a motif? Join the network! Trends Cell Biol. **11:** 315–318.

Depta, H., and Robinson, D.G. (1986). The isolation and enrichment of coated vesicles from suspension-cultured carrot cells. Protoplasma **130:** 162–170.

Dhonukshe, P., Aniento, F., Hwang, I., Robinson, D.G., Mravec, J., Stierhof, Y.-D., and Friml, J. (2007). Clathrin-mediated constitutive endocytosis of PIN auxin efflux carriers in *Arabidopsis*. Curr. Biol. **17:** 520–527.

Di Rubbo, S., et al. (2013). The clathrin adaptor complex AP-2 mediates endocytosis of BRASSINOSTEROID INSENSITIVE1 in *Arabidopsis*. Plant Cell **25:** 2986–2997.

Dong, J., MacAlister, C.A., and Bergmann, D.C. (2009). BASL controls asymmetric cell division in *Arabidopsis*. Cell **137:** 1320–1330.

Falbel, T.G., Koch, L.M., Nadeau, J.A., Seguí-Simarro, J.M., Sack, F.D., and Bednarek, S.Y. (2003). SCD1 is required for cytokinesis and polarized cell expansion in *Arabidopsis thaliana*. Development **130:** 4011–4024. Erratum. Development **130:** 4495.

Fan, L., Hao, H., Xue, Y., Zhang, L., Song, K., Ding, Z., Botella, M.A., Wang, H., and Lin, J. (2013). Dynamic analysis of *Arabidopsis* AP2 σ subunit reveals a key role in clathrin-mediated endocytosis and plant development. Development **140:** 3826–3837.

Fendrych, M., Synek, L., Pecenková, T., Drdová, E.J., Sekereš, J., de Rycke, R., Nowack, M.K., and Zársky, V. (2013). Visualization of the exocyst complex dynamics at the plasma membrane of *Arabidopsis thaliana*. Mol. Biol. Cell **24:** 510–520.

Fendrych, M., Synek, L., Pecenková, T., Toupalová, H., Cole, R.A., Drdová, E.J., Nebesárová, J., Sedinová, M., Hála, M., Fowler, J.E., and Zársky, V. (2010). The *Arabidopsis* exocyst complex is involved in cytokinesis and cell plate maturation. Plant Cell **22:** 3053–3065.

Fujimoto, M., Arimura, S., Ueda, T., Takanashi, H., Hayashi, Y., Nakano, A., and Tsutsumi, N. (2010). *Arabidopsis* dynamin-related proteins DRP2B and DRP1A participate together in clathrin-coated vesicle formation during endocytosis. Proc. Natl. Acad. Sci. USA **107:** 6094–6099.

Grosshans, B.L., Ortiz, D., and Novick, P.J. (2006). Rabs and their effectors: Achieving specificity in membrane traffic. Proc. Natl. Acad. Sci. USA **103:** 11821–11827.

Guseman, J.M., Lee, J.S., Bogenschutz, N.L., Peterson, K.M., Virata, R.E., Xie, B., Kanaoka, M.M., Hong, Z., and Torii, K.U. (2010). Dysregulation of cell-to-cell connectivity and stomatal patterning by loss-of-function mutation in *Arabidopsis* chorus (glucan synthase-like 8). Development **137:** 1731–1741.

Hála, M., Cole, R.A., Synek, L., Drdová, E.J., Pecenková, T., Nordheim, A., Lamkemeyer, T., Madlung, J., Hochholdinger, F., Fowler, J.E., and Zárský, V. (2008). An exocyst complex functions in plant cell growth in *Arabidopsis* and tobacco. Plant Cell **20:** 1330–1345.

Harley, S.M., and Beevers, L. (1989). Coated vesicles are involved in the transport of storage proteins during seed development in *Pisum sativum* L. Plant Physiol. **91:** 674–678.

Hayashi, M., Nito, K., Toriyama-Kato, K., Kondo, M., Yamaya, T., and Nishimura, M. (2000). AtPex14p maintains peroxisomal functions by determining protein targeting to three kinds of plant peroxisomes. EMBO J. **19:** 5701–5710.

Hruz, T., Laule, O., Szabo, G., Wessendorp, F., Bleuler, S., Oertle, L., Widmayer, P., Gruissem, W., and Zimmermann, P. (2008). Genevestigator v3: A reference expression database for the meta-analysis of transcriptomes. Adv. Bioinforma. **2008:** 420747.

Ingouff, M., Fitz Gerald, J.N., Guérin, C., Robert, H., Sørensen, M.B., Van Damme, D., Geelen, D., Blanchoin, L., and Berger, F. (2005). Plant formin AtFH5 is an evolutionarily conserved actin nucleator involved in cytokinesis. Nat. Cell Biol. **7:** 374–380.

Ito, E., Fujimoto, M., Ebine, K., Uemura, T., Ueda, T., and Nakano, A. (2012). Dynamic behavior of clathrin in *Arabidopsis thaliana* unveiled by live imaging. Plant J. **69:** 204–216.

Ivanova, Y., Smith, M.D., Chen, K., and Schnell, D.J. (2004). Members of the Toc159 import receptor family represent distinct pathways for protein targeting to plastids. Mol. Biol. Cell **15:** 3379–3392.

Jung, J.K.H., and McCouch, S. (2013). Getting to the roots of it: Genetic and hormonal control of root architecture. Front. Plant Sci. **4:** 186.

Kang, B.-H., Busse, J.S., and Bednarek, S.Y. (2003a). Members of the *Arabidopsis* dynamin-like gene family, ADL1, are essential for plant cytokinesis and polarized cell growth. Plant Cell **15:** 899–913.

Kang, B.-H., Busse, J.S., Dickey, C.E., Rancour, D.M., and Bednarek, S.Y. (2001). The Arabidopsis cell plate-associated dynamin-like protein, ADL1Ap, is required for multiple stages of plant growth and development. Plant Physiol. **126:** 47–68.

Kang, B.-H., Rancour, D.M., and Bednarek, S.Y. (2003b). The dynamin-like protein ADL1C is essential for plasma membrane maintenance during pollen maturation. Plant J. **35:** 1–15.

Kim, S.Y., Xu, Z.-Y., Song, K., Kim, D.H., Kang, H., Reichardt, I., Sohn, E.J., Friml, J., Juergens, G., and Hwang, I. (2013). Adaptor protein complex 2-mediated endocytosis is crucial for male reproductive organ development in *Arabidopsis*. Plant Cell **25:** 2970–2985.

Kirchhausen, T. (2000). Three ways to make a vesicle. Nat. Rev. Mol. Cell Biol. **1:** 187–198.

Kitakura, S., Vanneste, S., Robert, S., Löfke, C., Teichmann, T., Tanaka, H., and Friml, J. (2011). Clathrin mediates endocytosis and polar distribution of PIN auxin transporters in *Arabidopsis*. Plant Cell **23:** 1920–1931.

Klodmann, J., Senkler, M., Rode, C., and Braun, H.-P. (2011). Defining the protein complex proteome of plant mitochondria. Plant Physiol. **157:** 587–598.

Konopka, C.A., Backues, S.K., and Bednarek, S.Y. (2008). Dynamics of *Arabidopsis* dynamin-related protein 1C and a clathrin light chain at the plasma membrane. Plant Cell **20:** 1363–1380.

Konopka, C.A., and Bednarek, S.Y. (2008a). Comparison of the dynamics and functional redundancy of the Arabidopsis dynamin-related isoforms DRP1A and DRP1C during plant development. Plant Physiol. **147:** 1590–1602.

Konopka, C.A., and Bednarek, S.Y. (2008b). Variable-angle epifluorescence microscopy: A new way to look at protein dynamics in the plant cell cortex. Plant J. **53:** 186–196.

Korasick, D.A., McMichael, C.M., Walker, K.A., Anderson, J.C., Bednarek, S.Y., and Heese, A. (2010). Novel functions of Stomatal Cytokinesis-Defective 1 (SCD1) in innate immune responses against bacteria. J. Biol. Chem. **285:** 23342–23350.

Kouranti, I., Sachse, M., Arouche, N., Goud, B., and Echard, A. (2006). Rab35 regulates an endocytic recycling pathway essential for the terminal steps of cytokinesis. Curr. Biol. **16:** 1719–1725.

Laemmli, U.K. (1970). Cleavage of structural proteins during the assembly of the head of bacteriophage T4. Nature **227:** 680–685.

Lauber, M.H., Waizenegger, I., Steinmann, T., Schwarz, H., Mayer, U., Hwang, I., Lukowitz, W., and Jürgens, G. (1997). The *Arabidopsis* KNOLLE protein is a cytokinesis-specific syntaxin. J. Cell Biol. **139:** 1485–1493.

Lee, G.-J., Kim, H., Kang, H., Jang, M., Lee, D.W., Lee, S., and Hwang, I. (2007). EpsinR2 interacts with clathrin, adaptor protein-3, AtVTI12, and phosphatidylinositol-3-phosphate. Implications for EpsinR2 function in protein trafficking in plant cells. Plant Physiol. **143:** 1561–1575.

Lee, J.-H., Terzaghi, W., Gusmaroli, G., Charron, J.-B.F., Yoon, H.-J., Chen, H., He, Y.J., Xiong, Y., and Deng, X.W. (2008). Characterization of *Arabidopsis* and rice DWD proteins and their roles as substrate receptors for CUL4-RING E3 ubiquitin ligases. Plant Cell **20:** 152–167.

Leitner, J., Petrášek, J., Tomanov, K., Retzer, K., Pařezová, M., Korbei, B., Bachmair, A., Zažímalová, E., and Luschnig, C. (2012). Lysine63-linked ubiquitylation of PIN2 auxin carrier protein governs hormonally controlled adaptation of *Arabidopsis* root growth. Proc. Natl. Acad. Sci. USA **109:** 8322–8327.

Leonhardt, N., Kwak, J.M., Robert, N., Waner, D., Leonhardt, G., and Schroeder, J.I. (2004). Microarray expression analyses of *Arabidopsis* guard cells and isolation of a recessive abscisic acid hypersensitive protein phosphatase 2C mutant. Plant Cell **16:** 596–615.

Levivier, E., Goud, B., Souchet, M., Calmels, T.P.G., Mornon, J.-P., and Callebaut, I. (2001). uDENN, DENN, and dDENN: Indissociable domains in Rab and MAP kinases signaling pathways. Biochem. Biophys. Res. Commun. **287:** 688–695.

Li, Y., Rosso, M.G., Viehoever, P., and Weisshaar, B. (2007). GABI-Kat SimpleSearch: An *Arabidopsis thaliana* T-DNA mutant database with detailed information for confirmed insertions. Nucleic Acids Res. **35** (Database issue)**:** D874–D878.

Li, Y., Shen, Y., Cai, C., Zhong, C., Zhu, L., Yuan, M., and Ren, H. (2010). The type II *Arabidopsis* formin14 interacts with microtubules and microfilaments to regulate cell division. Plant Cell **22:** 2710–2726.

MacAlister, C.A., Ohashi-Ito, K., and Bergmann, D.C. (2007). Transcription factor control of asymmetric cell divisions that establish the stomatal lineage. Nature **445:** 537–540.

Marat, A.L., Dokainish, H., and McPherson, P.S. (2011). DENN domain proteins: Regulators of Rab GTPases. J. Biol. Chem. **286:** 13791–13800.

Marat, A.L., Ioannou, M.S., and McPherson, P.S. (2012). Connecdenn 3/DENND1C binds actin linking Rab35 activation to the actin cytoskeleton. Mol. Biol. Cell **23:** 163–175.

Marat, A.L., and McPherson, P.S. (2010). The connecdenn family, Rab35 guanine nucleotide exchange factors interfacing with the clathrin machinery. J. Biol. Chem. **285:** 10627–10637.

McDonnell, A.V., Jiang, T., Keating, A.E., and Berger, B. (2006). Paircoil2: Improved prediction of coiled coils from sequence. Bioinformatics **22:** 356–358.

McMichael, C.M., and Bednarek, S.Y. (2013). Cytoskeletal and membrane dynamics during higher plant cytokinesis. New Phytol. **197:** 1039–1057.

Murashige, T., and Skoog, F. (1962). A revised medium for rapid growth and biological assays with tobacco tissue cultures. Physiol. Plant. **15:** 473–497.

Nadeau, J.A. (2009). Stomatal development: New signals and fate determinants. Curr. Opin. Plant Biol. **12:** 29–35.

Nakamura, R.L., McKendree, W.L., Jr., Hirsch, R.E., Sedbrook, J.C., Gaber, R.F., and Sussman, M.R. (1995). Expression of an Arabidopsis potassium channel gene in guard cells. Plant Physiol. **109:** 371–374.

Novick, P.J., Ferro, S., and Schekman, R. (1981). Order of events in the yeast secretory pathway. Cell **25:** 461–469.

Novick, P.J., Field, C., and Schekman, R. (1980). Identification of 23 complementation groups required for post-translational events in the yeast secretory pathway. Cell **21:** 205–215.

Park, M., Song, K., Reichardt, I., Kim, H., Mayer, U., Stierhof, Y.-D., Hwang, I., and Jürgens, G. (2013). *Arabidopsis* μ-adaptin subunit AP1M of adaptor protein complex 1 mediates late secretory and vacuolar traffic and is required for growth. Proc. Natl. Acad. Sci. USA **110:** 10318–10323.

Patino-Lopez, G., Dong, X., Ben-Aissa, K., Bernot, K.M., Itoh, T., Fukuda, M., Kruhlak, M.J., Samelson, L.E., and Shaw, S. (2008). Rab35 and its GAP EPI64C in T cells regulate receptor recycling and immunological synapse formation. J. Biol. Chem. **283:** 18323–18330.

Pellinen, T., et al. (2008). Integrin trafficking regulated by Rab21 is necessary for cytokinesis. Dev. Cell **15:** 371–385.

Pillitteri, L.J., Sloan, D.B., Bogenschutz, N.L., and Torii, K.U. (2007). Termination of asymmetric cell division and differentiation of stomata. Nature **445:** 501–505.

Preuss, M.L., Serna, J., Falbel, T.G., Bednarek, S.Y., and Nielsen, E. (2004). The *Arabidopsis* Rab GTPase RabA4b localizes to the tips of growing root hair cells. Plant Cell **16:** 1589–1603.

Punta, M., Coggill, P.C., Eberhardt, R.Y., Mistry, J., Tate, J., Boursnell, C., Pang, N., Forslund, K., Ceric, G., Clements, J., Heger, A., Holm, L., Sonnhammer, E.L., Eddy, S.R., Bateman, A., and Finn, R.D. (2012). The Pfam protein families database. Nucleic Acids Res. Nucleic Acids Res. **40:** D290–D301.

Rancour, D.M., Dickey, C.E., Park, S., and Bednarek, S.Y. (2002). Characterization of AtCDC48. Evidence for multiple membrane fusion mechanisms at the plane of cell division in plants. Plant Physiol. **130:** 1241–1253.

Robert, S., et al. (2010). ABP1 mediates auxin inhibition of clathrin-dependent endocytosis in *Arabidopsis*. Cell **143:** 111–121.

Rounds, C.M., Lubeck, E., Hepler, P.K., and Winship, L.J. (2011). Propidium iodide competes with Ca(2+) to label pectin in pollen tubes and Arabidopsis root hairs. Plant Physiol. **157:** 175–187.

Rutherford, S., and Moore, I. (2002). The *Arabidopsis* Rab GTPase family: Another enigma variation. Curr. Opin. Plant Biol. **5:** 518–528.

Sato, M., Sato, K., Liou, W., Pant, S., Harada, A., and Grant, B.D. (2008). Regulation of endocytic recycling by *C. elegans* Rab35 and its regulator RME-4, a coated-pit protein. EMBO J. **27:** 1183–1196.

Schneider, C.A., Rasband, W.S., and Eliceiri, K.W. (2012). NIH Image to ImageJ: 25 years of image analysis. Nat. Methods **9:** 671–675.

Servant, F., Bru, C., Carrère, S., Courcelle, E., Gouzy, J., Peyruc, D., and Kahn, D. (2002). ProDom: Automated clustering of homologous domains. Brief. Bioinform. **3:** 246–251.

Smith, L.G. (2003). Cytoskeletal control of plant cell shape: Getting the fine points. Curr. Opin. Plant Biol. **6:** 63–73.

Song, J., Lee, M.H., Lee, G.-J., Yoo, C.M., and Hwang, I. (2006). *Arabidopsis* EPSIN1 plays an important role in vacuolar trafficking of soluble cargo proteins in plant cells via interactions with clathrin, AP-1, VTI11, and VSR1. Plant Cell **18:** 2258–2274.

Song, K., Jang, M., Kim, S.Y., Lee, G., Lee, G.-J., Kim, D.H., Lee, Y., Cho, W., and Hwang, I. (2012). An A/ENTH domain-containing protein functions as an adaptor for clathrin-coated vesicles on the growing cell plate in Arabidopsis root cells. Plant Physiol. **159:** 1013–1025.

Strand, Å., Zrenner, R., Trevanion, S., Stitt, M., Gustafsson, P., and Gardeström, P. (2000). Decreased expression of two key enzymes in the sucrose biosynthesis pathway, cytosolic fructose-1,6-bisphosphatase and sucrose phosphate synthase, has remarkably different consequences for photosynthetic carbon metabolism in transgenic *Arabidopsis thaliana*. Plant J. **23:** 759–770.

Strompen, G., Dettmer, J., Stierhof, Y.-D., Schumacher, K., Jürgens, G., and Mayer, U. (2005). *Arabidopsis* vacuolar H-ATPase subunit E isoform 1 is required for Golgi organization and vacuole function in embryogenesis. Plant J. **41:** 125–132.

Synek, L., Schlager, N., Eliás, M., Quentin, M., Hauser, M.-T., and Zárský, V. (2006). AtEXO70A1, a member of a family of putative exocyst subunits specifically expanded in land plants, is important for polar growth and plant development. Plant J. **48:** 54–72.

Szymkiewicz, I., Shupliakov, O., and Dikic, I. (2004). Cargo- and compartment-selective endocytic scaffold proteins. Biochem. J. **383:** 1–11.

Teh, O.-K., Shimono, Y., Shirakawa, M., Fukao, Y., Tamura, K., Shimada, T., and Hara-Nishimura, I. (2013). The AP-1 μ adaptin is required for KNOLLE localization at the cell plate to mediate cytokinesis in *Arabidopsis*. Plant Cell Physiol. **54:** 838–847.

Thellmann, M., Rybak, K., Thiele, K., Wanner, G., and Assaad, F.F. (2010). Tethering factors required for cytokinesis in Arabidopsis. Plant Physiol. **154:** 720–732.

Thiele, K., Wanner, G., Kindzierski, V., Jürgens, G., Mayer, U., Pachl, F., and Assaad, F.F. (2009). The timely deposition of callose is essential for cytokinesis in *Arabidopsis*. Plant J. **58:** 13–26.

Töller, A., Brownfield, L., Neu, C., Twell, D., and Schulze-Lefert, P. (2008). Dual function of *Arabidopsis* glucan synthase-like genes GSL8 and GSL10 in male gametophyte development and plant growth. Plant J. **54:** 911–923.

Van Damme, D., Coutuer, S., De Rycke, R., Bouget, F.-Y., Inzé, D., and Geelen, D. (2006). Somatic cytokinesis and pollen maturation in *Arabidopsis* depend on TPLATE, which has domains similar to coat proteins. Plant Cell **18:** 3502–3518.

Van Damme, D., Gadeyne, A., Vanstraelen, M., Inzé, D., Van Montagu, M.C.E., De Jaeger, G., Russinova, E., and Geelen, D. (2011). Adaptin-like protein TPLATE and clathrin recruitment during plant somatic cytokinesis occurs via two distinct pathways. Proc. Natl. Acad. Sci. USA **108:** 615–620.

Verbelen, J.-P., De Cnodder, T., Le, J., Vissenberg, K., and Baluška, F. (2006). The root apex of *Arabidopsis thaliana* consists of four distinct zones of growth activities: Meristematic zone, transition zone, fast elongation zone and growth terminating zone. Plant Signal. Behav. **1:** 296–304.

Wang, C., Yan, X., Chen, Q., Jiang, N., Fu, W., Ma, B., Liu, J., Li, C., Bednarek, S.Y., and Pan, J. (2013). Clathrin light chains regulate clathrin-mediated trafficking, auxin signaling, and development in *Arabidopsis*. Plant Cell **25:** 499–516.

Wang, Y., Zhang, X., Zhang, H., Lu, Y., Huang, H., Dong, X., Chen, J., Dong, J., Yang, X., Hang, H., and Jiang, T. (2012). Coiled-coil networking shapes cell molecular machinery. Mol. Biol. Cell **23:** 3911–3922.

Winter, D., Vinegar, B., Nahal, H., Ammar, R., Wilson, G.V., and Provart, N.J. (2007). An "Electronic Fluorescent Pictograph" browser for exploring and analyzing large-scale biological data sets. PLoS ONE **2:** e718.

Yamaoka, S., Shimono, Y., Shirakawa, M., Fukao, Y., Kawase, T., Hatsugai, N., Tamura, K., Shimada, T., and Hara-Nishimura, I. (2013). Identification and dynamics of *Arabidopsis* adaptor protein-2 complex and its involvement in floral organ development. Plant Cell **25:** 2958–2969.

Yang, M., Nadeau, J.A., Zhao, L., and Sack, F.D. (1999). Characterization of a cytokinesis defective (cyd1) mutant of *Arabidopsis*. J. Exp. Bot. **50:** 1437–1446.

Ye, J., Zheng, Y., Yan, A., Chen, N., Wang, Z., Huang, S., and Yang, Z. (2009). *Arabidopsis* formin3 directs the formation of actin cables and polarized growth in pollen tubes. Plant Cell **21:** 3868–3884.

Yoshimura, S., Gerondopoulos, A., Linford, A., Rigden, D.J., and Barr, F.A. (2010). Family-wide characterization of the DENN domain Rab GDP-GTP exchange factors. J. Cell Biol. **191:** 367–381.

Zhang, J., Fonovic, M., Suyama, K., Bogyo, M., and Scott, M.P. (2009). Rab35 controls actin bundling by recruiting fascin as an effector protein. Science **325:** 1250–1254.